**Glycobiology** vol. 10 no. 10 pp. 959–974, 2000

# Molecular dynamics simulation of human prion protein including both N-linked oligosaccharides and the GPI anchor

**Johannes Zuegg and Jill E.Gready[1]**

Division of Biochemistry and Molecular Biology, John Curtin School of Medical Research, Australian National University, P.O. Box 334, Canberra, ACT 2601, Australia

*Received on December 16, 1999; revised on April 11, 2000; accepted on April 18, 2000*

**Although glycosylation appears to protect prion protein ($PrP^C$) from the conformational transition to the disease-associated scrapie form ($PrP^{Sc}$), available NMR structures are for non-glycosylated $PrP^C$, only. To investigate the influence of both the two N-linked glycans, Asn181 and Asn197, and of the GPI anchor attached to Ser230, on the structural, dynamical and electrostatic behavior of PrP, we have undertaken molecular dynamics simulations on the C-terminal region of human prion protein *Hu*PrP(90–230), with and without the three glycans. The simulations used the AMBER94 force field in a periodic box model with explicit water molecules, considering all long-range electrostatic interactions. The results suggest the structured part of the protein, *Hu*PrP(127–227) is stabilized overall from addition of the glycans, specifically by extensions of Helix-B and Helix-C and reduced flexibility of the linking turn containing Asn197, although some regions such as residues in the turn (165–170) between Strand-B and Helix-B have increased flexibility. The stabilization appears indirect, by reducing the mobility of the surrounding water molecules, and not from specific interactions such as H bonds or ion pairs. The results are consistent with glycosylation at Asn197 having a stabilizing role, while that at Asn181, in a region with already stable secondary structure, having a more functional role, in agreement with literature suggestions. Due to three negatively charged $SiaLe^x$ groups per N-glycan, the surface electrostatic properties change to a negative electrostatic field covering most of the C-terminal part, including the surface of Helix-B and Helix-C, while the positively charged N-terminal part PrP(90–126) of undefined structure creates a positive potential. The unusual hydrophilic Helix-A (144–152) is not covered by either of these dominant electrostatic fields, and modeling shows it could readily dimerize in anti parallel fashion. In combination with separate simulations of the GPI anchor in a membrane model, the results show the GPI anchor is highly flexible and would maintain the protein at a distance between 9 and 13 Å from the membrane surface, with little influence on its structure or orientational freedom.**

*Key words:* human prion protein/N-linked glycan/GPI anchor/molecular dynamics/conformation

## Introduction

Prion protein (PrP) is associated with an unusual class of neurodegenerative diseases, which includes scrapie in sheep; bovine spongiform encephalopathy (BSE) in cattle; and kuru, Creutzfeldt-Jacob disease (CJD), Gerstmann-Sträussler-Scheinker syndrome (GSS), and fatal familiar insomnia (FFI) in humans (Prusiner, 1996; Edenhofer *et al.*, 1997; Ironside, 1998). According to the *protein-only* hypothesis (Prusiner, 1982, 1998) the disease is caused by an abnormal form of the 250 amino acid PrP, which accumulates in plaques in the brain. The protein component of this disease-associated form of PrP ($PrP^{Sc}$) differs from the normal cellular form ($PrP^C$) only in its 3-D structure, and FTIR and CD spectra indicate it has a significantly increased content of β-sheet conformation compared with $PrP^C$ (Pan *et al.*, 1993; Horwich and Weissman, 1997). $PrP^C$ is a secreted cell surface glycoprotein with still unknown function, which cycles between the cell surface and endocytic compartments (Shyng *et al.*, 1993; Vey *et al.*, 1996; Harris, 1999). The accumulation of $PrP^{Sc}$ occurs in late endosomes and lysosomes (Arnold *et al.*, 1995). The conformational change between $PrP^C$ and $PrP^{Sc}$ in animals and humans is strongly associated with mutations in the PrP gene and leads to a protease-resistant remnant consisting of the residues 90–231, which appears to be the minimum unit correlated with infectivity. So far, 17 disease-associated mutations of PrP are known for humans (Ironside, 1998; Zuegg and Gready, 1999), most of which occur in the second half of the C-terminal region.

The mature form of $PrP^C$, made up of residues 23–231, is anchored to the cell membrane via a glycosyl-phosphatidyl-inositol anchor (GPI anchor) at its C terminus (Stahl *et al.*, 1987, 1992; Baldwin *et al.*, 1993), and has one disulfide bridge ($Cys^{179}$-$Cys^{214}$; human numbering). In addition, mammalian PrP contains two consensus sites for N-linked glycosylation, at $Asn^{181}$ and $Asn^{197}$ of human PrP (*Hu*PrP) and Syrian hamster PrP (*Sh*PrP), and at $Asn^{180}$ and $Asn^{196}$ in murine PrP (*Mo*PrP). Studies of the N-linked glycans of *Mo*PrP (Stimson *et al.*, 1999) and *Sh*PrP (Endo *et al.*, 1989; Rudd *et al.*, 1999a) have shown that both sites are occupied and that they contain up to 60 different but overlapping sets of sugars, including charged sialyl-Lewis$^x$ ($SiaLe^x$) epitopes, which are suggested to serve as cell-surface recognition molecules (Eggens *et al.*, 1989; Bevilacqua *et al.*, 1991).

[1]To whom correspondence should be addressed at: Division of Biochemistry and Molecular Biology, John Curtin School of Medical Research, Australian National University, P.O. Box 334, Canberra, ACT 2601, Australia

NMR structures of the full-length and N-terminally truncated forms of recombinant *Mo*PrP (Riek *et al.*, 1996; Billeter *et al.*, 1997; Riek *et al.*, 1997; Riek *et al.*, 1998), *Sh*PrP (Donne *et al.*, 1997; James *et al.*, 1997; Liu *et al.*, 1999), and *Hu*PrP (Hosszu *et al.*, 1999; Zahn *et al.*, 2000) have revealed that the whole N-terminal segment $PrP^{23–126}$ is flexibly disordered and that only the C-terminal part $PrP^{127–231}$ possesses a defined 3-D structure. The structurally well-defined part of PrP consists of three α-helices and a small two-stranded antiparallel β-sheet. All NMR studies could identify the three α-helices, although with slightly different lengths, but showed differences for the antiparallel β-sheet, which was not always as well defined (Donne *et al.*, 1997; James *et al.*, 1997; Hosszu *et al.*, 1999).

The biological roles of oligosaccharides of glycoproteins are as diverse as their structures, and include cell surface signaling, cell recognition, intracellular trafficking, secretion, stabilizing and protecting tertiary protein structure, regulating activity of enzymes, and clearance and turnover of the glycoproteins (Varki, 1993). In addition, oligosaccharides are so flexible in their 3-D structures that even NMR experiments can rarely define their structural and dynamical properties unambiguously (Peters and Pinto, 1996). Recent reports indicate combining NMR and x-ray crystallography can help to identify the structures of oligosaccharides on proteins, at least for the first five to six sugar residues (Rudd *et al.*, 1999b). The great variety of possible functions combined with the structurally flexible nature of oligosaccharides makes elucidation of structure–activity relationships very difficult, especially given the lack of experimental tools to characterize the structural and dynamical properties of oligosaccharides linked to proteins. Molecular dynamics (MD) simulations alone (Barboni *et al.*, 1995; Woods *et al.*, 1995; Naidoo *et al.*, 1997), or in combination with NMR (Agrawal *et al.*, 1999; Rudd *et al.*, 1999c), have proven to be a valuable tool for assessing the flexibility of oligosaccharides. However, all NMR studies with PrP were done with protein lacking both N-linked glycans and GPI anchor. Hence, in order to identify a possible role for the glycosylation of mammalian PrP, we have undertaken MD simulations and analyzed the structure and flexibility of the PrP glycans, and their influence on the protein structure.

We have recently undertaken MD simulations with nonglycosylated models of $ShPrP^{90–231}$ and $HuPrP^{90–230}$ (Zuegg and Gready, 1999). These revealed that correct treatment of the long-range electrostatic interactions was necessary to get stable trajectories. This requirement was attributed to the relatively high number of charged residues on the surface of PrP and the fact that the protein has different regions with distinct electrostatic properties. $PrP^{90–230}$ consists of an N-terminal part with only positively charged residues ($PrP^{90–112}$), a hydrophobic part with no charged residues at all ($PrP^{113–133}$), and a C-terminal part with a large number of positively and negatively charged residues ($PrP^{134–230}$). Only by considering all long-range electrostatic interactions using the particle mesh Ewald (PME) method (Darden *et al.*, 1993), could trajectories with low root mean square deviation (RMSD) and with stable secondary structure be generated. However, the simulations showed some flexibility in the *structured* part of PrP, $PrP^{127–230}$, leading to shortened α-helical structure and in some cases even to a split in the third α-helix (Helix-C). In this paper we investigate the influence on the structure of PrP of glycosylation of the two N-glycosylation sites, by comparing the results of MD simulations of the *Hu*PrP homology model with results of simulations of *Hu*PrP with both N-glycans attached. Also, in order to define possible orientations of PrP with respect to the membrane, the oligosaccharide part of the GPI anchor bonded to the C-terminal $Ser^{230}$ was included in the model. To identify a possible distance between PrP and the membrane, the results of these MD simulations of the fully glycosylated *Hu*PrP model (glyc-*Hu*PrP) were combined with simulations of a membrane model which included just the GPI anchor. Finally, we have compared the dynamic and structural behavior of the glycans when bound to PrP with results of simulations of their free, solvated forms. This allows assessment of any restrictions on the flexibility of the glycans by the protein environment.

## Results

### *Model for the N-linked glycans and GPI anchor*

The two N-linked glycans were considered to be the same for both N-glycosylation sites, $Asn^{181}$ and $Asn^{197}$, and to consist of the largest and most charged oligosaccharide possible. Thus, the model used for the oligosaccharide, as shown in Figure 1, consists of a tetraantennary glycan with two negatively charged sialyl-$Lewis^x$ epitopes (NeuNAcα(2–3)Galβ(1–4)(Fuc-α(1–3))GlcNAc), one negatively charged NeuNAcα(2–6)Galβ(1–4)GlcNAc group and one neutral Galβ(1–4)GlcNAc group as the four antennas. This model, with an overall charge of –3 e.u., can be considered the glycan from which all the oligosaccharides found by experiment

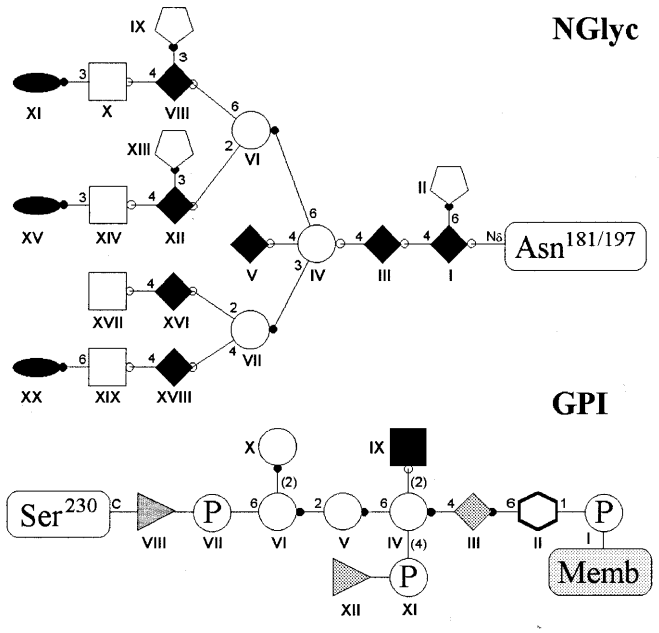


**Fig. 1.** Schematic representation of the oligosaccharide models for the N-linked glycan (NGlyc) and the GPI anchor (GPI). Open circles, Man; solid diamonds, GlcNAc; open pentagons, Fuc; open squares, Gal; solid ovals, NeuNAc; open hexagons, *m*Ino; solid squares, GalNAc; shaded diamonds, GlcN; circled Ps, $PO_2$; shaded triangles, Ethanolamine; filled circles with lines, α-anomer; open circles with lines, β-anomer. Roman numbering indicates the residues number. Arabic numbers indicate the linkage type of the glycosidic linkage, while numbers in parenthesis indicate the linkage type used by analogy to the rat Thy-1 protein (McConville and Ferguson, 1993).

(Endo *et al.*, 1989; Rudd *et al.*, 1999a; Stimson *et al.*, 1999) can be derived by partial degradation.

For the GPI anchor, experiments could not give an unequivocal structure for the glycan (Stahl *et al.*, 1992; Baldwin *et al.*, 1993). Therefore, the GPI-anchor model used, also shown in Figure 1, consists of the core linkage chain between the protein and the phosphoinositol, and branches built by analogy with the GPI anchor of the rat Thy-1 protein (McConville and Ferguson, 1993). In comparison with the largest structure found by experiment (Baldwin *et al.*, 1993), the model is lacking a NeuNAc-Gal group attached to the GalNAc residue, for which neither the type of glycosidic linkage nor the anomeric type could be identified. The overall charge of the GPI model was –1 e.u., with all -$NH_2$ groups of ethanolamine and GlcN being considered protonated, and all the -$PO_2$- groups in their anionic form.

*Protein structure comparison between HuPrP and glyc-HuPrP*

Both *Hu*PrP models, with (glyc-*Hu*PrP) and without the oligosaccharides (*Hu*PrP), were simulated with the same parameters and for the same time of ~2 ns (see Table I). Comparison of the RMSDs of the backbone atoms of both models from their common starting conformation shows that even though the RMSD for the whole protein ($PrP^{90\text{-}231}$) is higher for the glycosylated model, the RMSDs of the structured part of the protein $PrP^{127–227}$ are the same in both simulations (see Figure 2). The higher RMSD of the glycosylated model is due to different conformations of the N-terminal part of the protein ($PrP^{90\text{-}126}$) only. The RMSDs of the oligosaccharides in glyc-*Hu*PrP are between 3.7 and 5.1 Å, i.e., higher than the RMSD of the protein backbone of the structured part (2.1Å) but still considerably lower than the RMSD of the flexible N-terminal part (11.8 Å) (see Table I). Of the three oligosaccharides, $NGlyc^{197}$ shows the highest RMSD (5.1 Å). Secondary structure analysis, shown in Figure 3, indicates increased stability of the α-helical structure for the glycosylated model. The two C-terminal α-helices, B and C, show increased lengths which resemble more the NMR structure of *Sh*PrP (Liu *et al.*, 1999), although Helix-C is still shorter by 3 residues at its C-terminal end. In addition, no splitting of Helix-C could be seen in the glycosylated model in contrast to the *Hu*PrP model (Zuegg and Gready, 1999). The flexibility of the backbone, shown in Figure 3 as standard deviation (SD) of the ϕ and ψ backbone torsion angles and in Figure 4 as the radius of the coil tracing the positions of the Cα atoms, decreases significantly for the residues around the $N^{197}$ glycosylation site in Turn-D, but remain similar throughout the other parts of the protein. However, the Turn-C region, $PrP^{165–170}$, in the glyc-*Hu*PrP model shows a slightly increased flexibility. The average structures for both simulations are also very similar (see Figure 4), even though the RSMD of the backbone atoms between both structures is calculated to be 2.5 Å. The main differences between the two structures are of slightly different conformations for turns A, C, and D. Turn-D is at the $N^{197}$ glycosylation site and, therefore, influenced by $NGlyc^{197}$, but the other two turns are not directly influenced by the glycans. The intraprotein interactions are also similar for both models. The three major salt bridges, $Glu^{146}\leftrightarrow Arg^{208}$, $Arg^{164}\leftrightarrow Asp^{178}$ and $Arg^{156}\leftrightarrow Glu^{196}$ (Zuegg and Gready, 1999), are present in both simulations for more than 90% of the time (see Table II). The exception is the salt bridge $Arg^{156}\leftrightarrow Glu^{196}$, between Helix-A and Turn-D, for which the occupancy drops in the glyc-*Hu*PrP simulation to 78.4 %, due to the proximity of the $N^{197}$ glycan.

**Table I.** MD simulation conditions and results

| | *Hu*PrP | glyc-*Hu*PrP |
|---|---|---|
| Atoms | 2180 | 3376 |
| Molecular mass (kDa) | 16.0 | 25.3 |
| $Cl^-$, $Na^+$ ions | 13, 12 | 15, 20 |
| Water molecules | 5143 | 10321 |
| Box size (Å) | 61 × 58 × 53 | 65 × 80 × 72 |
| Simulation time (ps) | 2300 | 1800 |
| RMSD[a,b] (Å) | | |
| All (90–231) | 5.0 | 7.6 |
| N-Terminus (90–126) | 7.1 | 11.8 |
| Structured (127–227) | 2.4 | 2.1 |
| $NGlyc^{181}$, $NGlyc^{197}$ | — | 4.9, 5.1 |
| GPI | — | 3.7 |
| SD (torsion angles)[a,c] (°) | | |
| All (90–231) | 18.4 | 18.8 |
| N-Terminus (90–126) | 26.5 | 31.5 |
| Structured (127–227) | 15.3 | 13.7 |
| $NGlyc^{181}$, $NGlyc^{197}$ | | 17.2, 21.3 |
| GPI | | 28.1 |
| Secondary structure[a](%) | | |
| α-Helix | 35.1 | 38.8 |
| $3_{10}$-Helix | 11.4 | 6.1 |
| β-Strand | 4.0 | 3.1 |
| H-Bonded turn | 18.9 | 15.7 |
| | solv-NGlyc | solv-GPI |
| Atoms | 513 | 191 |
| Molecular mass (kDa) | 3.7 | 1.5 |
| $Cl^-$, $Na^+$ ions | 0, 3 | 1, 1 |
| Water molecules | 3132 | 1120 |
| Box size (Å) | 42 × 57 × 44 | 30 × 32 × 38 |
| Simulation time (ps) | 1300 | 1000 |
| RMSD[a,b] (Å) | 6.3 | 4.0 |
| SD (torsion angles)[a,c] (°) | 20.1 | 29.6 |
| | cho-GPI | cho-GPI |
| Atoms (GPI+Memb) | 6755 | 5837 |
| $Cl^-$, $Na^+$ ions | 0, 1 | 0, 1 |
| Water molecules | 1107 | 1244 |
| Cap radius (Å) | 30 | 30 |
| Simulation time (ps) | 1000 | 1000 |
| RMSD[a,b] (Å) | 3.5 | 3.4 |
| SD (torsion angles)[a,c] (°) | 31.2 | 27.7 |

[a]Corresponding average values over the whole simulation.
[b]RMSD of protein backbone atoms, or heavy atoms of the oligosaccharides.
[c]ϕ and ψ backbone torsion angles for protein, and ϕ, ψ and ω torsion angles of glycosidic linkage.

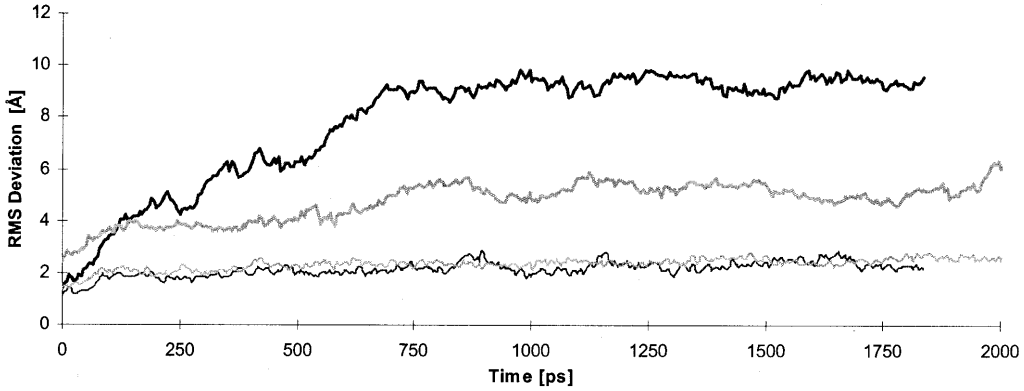


**Fig. 2.** Root mean square deviation (RMSD) of the backbone atom positions from their starting positions as a function of time, for simulations of the *Hu*PrP (gray line) and glyc-*Hu*PrP models (solid line). The RMSD is shown in both cases for the whole model $PrP^{90-230}$ as a thick line, and for the *structured* part of the protein $PrP^{127–227}$ as a thin line.

**Table II.** Salt bridges from the simulations of *Hu*PrP and glyc-*Hu*PrP, shown as percentage occupancy during the whole simulation

| Salt bridges[a] | | *Hu*PrP | glyc- *Hu*PrP |
|---|---|---|---|
| Negative | Positive | | |
| Asp144 ($\alpha_A$) | His140 ($\tau_A$) | 66.9 | 36.4 |
| Asp144 ($\alpha_A$) | Arg148 ($\alpha_A$) | 68.5 | 26.7 |
| Glu146 ($\alpha_A$) | Arg208 ($\alpha_C$) | 97.5 | 100.0 |
| Asp147 ($\alpha_A$) | Arg151 ($\alpha_A$) | 9.6 | 94.0 |
| Asp147 ($\alpha_A$) | His140 ($\tau_A$) | 71.9 | 83.8 |
| Glu152 ($\alpha_A$) | Arg148 ($\alpha_A$) | 1.4 | 57.2 |
| Asp178 ($\alpha_B$) | Arg164 ($\tau_C$) | 90.4 | 98.2 |
| Glu196 ($\tau_D$) | Arg156 ($\alpha_A$) | 96.9 | 78.4 |
| Glu207 ($\alpha_C$) | Lys204 ($\alpha_C$) | 95.9 | 89.7 |
| Glu211 ($\alpha_C$) | His177 ($\alpha_B$) | 23.4 | — |
| Glu221 ($\alpha_C$) | Arg220 ($\alpha_C$) | 25.8 | 37.8 |

[a]The average secondary structure elements, corresponding to the glyc-*Hu*PrP simulation, are shown in parentheses. Underlined residues are residues for which mutation is known to be associated with CJD, GSS, or FFI in humans.

The salt bridges in the Helix-A region on the other hand, $Asp^{144}$↔$His^{140}$, $Asp^{144}$↔$Arg^{148}$, $Asp^{147}$↔$Arg^{151}$ and $Glu^{152}$↔$Arg^{148}$, which involve only neighboring residues (e.g., ± 4), are somewhat reorganized, with some increasing and others decreasing their occupancies. Differences in the occupancies between this work and previous work (Zuegg and Gready, 1999) are due only to a longer simulation time (2300 ps compared with 720 ps). The H-bond network is also similar between the two simulations with similar overall number of H-bonds (see Table III).

The flexible N-terminal part of PrP, $PrP^{90-126}$, shows high flexibility and no unique structure in both models. For the glyc-*Hu*PrP model this region exhibits a greater conformational change, including a higher RMSD and increased flexibility of the backbone torsion angles, with an average SD of 31.5°, compared with 26.5° for the *Hu*PrP model. Both N-linked glycans appear to influence the position of this N-terminal part, with a different orientation compared with the simulation without oligosaccharides, and with no evidence of α-helical structure in the $PrP^{111–118}$ region (Zuegg and Gready, 1999) except for a small amount of $3_{10}$-helical structure occurring transiently.

*Structure and dynamics of glycans*

As may be seen in Figure 4, the simulation of the glycosylated *Hu*PrP model showed no unique orientation for either NGlyc chain. With a RMSD of the heavy atoms of $NGlyc^{181}$ and $NGlyc^{197}$ from the starting conformation of 4.9 and 5.1 Å, respectively, and an average SD of the glycosidic linkage torsion angles (ϕ and ψ, and ω in the case of a 1–6 linkage) of 17.2° and 21.3°, respectively, both N-glycans exhibit high flexibility. These SD values for the torsion angles are similar to the value of 20.1° from the simulation of the free NGlyc model in solution (see Table I). Nevertheless, the N-linked glycans seem to be slightly restricted by the protein, as the core of the glycan, formed by $Man^{VI}$-($Man^{VII}$-)$Man^{IV}$-$GlcNAc^{III}$-$GlcNAc^{I}$-$Asn^{181/197}$, seems to have reduced flexibility compared with the simulation of the solution structure, especially for the usually highly flexible 1→6 linkage of $Man^{VI}$-$Man^{IV}$ (see Figure 5). Compared with the core structure, the four antennas of the NGlyc models have high flexibility, especially both $SiaLe^x$ groups of the $N^{197}$-linked glycan show high flexibility compared with those in the $NGlyc^{181}$ glycan. Generally, $NGlyc^{197}$ has higher flexibility than $NGlyc^{181}$, as can be seen in the higher SD of the torsion angles.

The GPI anchor shows similar behavior to that of the NGlyc structures. In the glyc-*Hu*PrP simulation the SD for the torsion angles of the GPI model is 28.1°, similar to that for the solvated model (solv-GPI) with 29.6°. The heavy-atom RMSDs 3.7 and 4.0Å, respectively, are also similar. As for the NGlyc chains, a core structure with reduced flexibility can be identified in the GPI anchor, consisting of $Man^{V}$-$Man^{IV}$-$GlcN^{III}$-*m*$Ino^{II}$. This part also showed some NOE interactions in NMR experiments with solvated forms of similar GPI anchors (Homans *et al.*, 1989; Weller *et al.*, 1994). The average distances in the glyc-*Hu*PrP and solv-GPI simulations for *m*$Ino^{II}$-H6↔$GlcN^{III}$-H1 and $Man^{IV}$-H1↔$GlcN^{III}$-H4, shown in Table IV, are in good agreement with the experimental values. The remaining NOE interactions are not quite as consistent, as

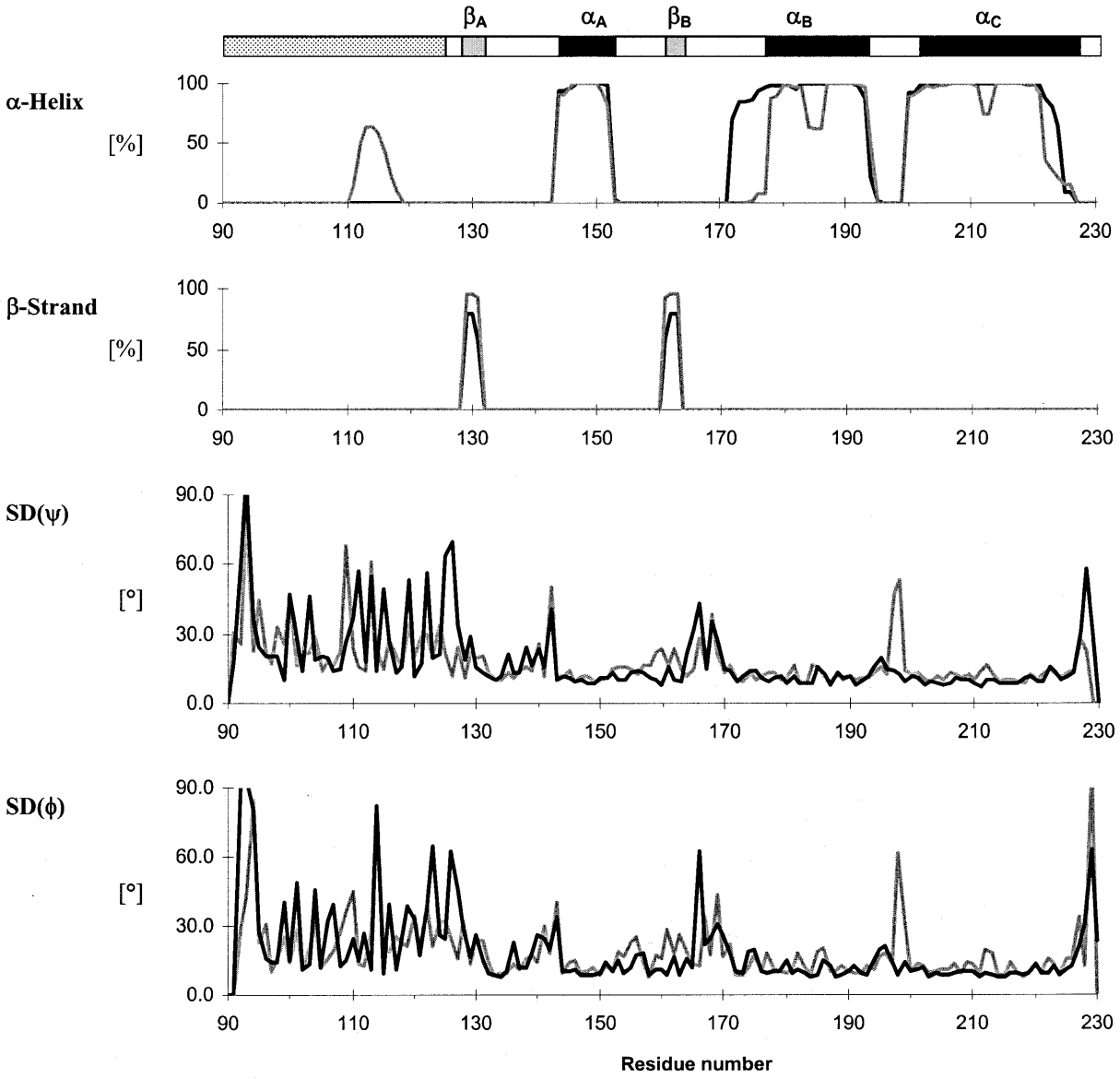


**Fig. 3.** Secondary structure (α-helix and β-sheets) per residue averaged over the complete simulation and standard deviation (SD) of the backbone torsion angles, ϕ and ψ, for the *Hu*PrP (gray lines) and glyc-*Hu*PrP (black lines) simulations. Secondary structure bar at top shows the average secondary structure of the glyc-*Hu*PrP simulation (solid bar for α-helices, gray bar for β-sheets, and stippled bar for the flexible region).

the branching at $Man^{IV}$ of the GPI anchors used in the NMR experiments differs significantly from that used in the simulations. The linkage to PrP, $Ser^{230}$-$Ea^{VIII}$-$PO_2^{VII}$-$Man^{VI}$, is less flexible than in the solv-GPI simulation but still too flexible to give a unique overall conformation for the GPI anchor. When coupled with the highly flexible C-terminal part of PrP, $PrP^{228–230}$, this makes it impossible to identify a precise orientation for the anchor point into a membrane.

*Orientation and interaction between glycans and protein*

In the glyc-*Hu*PrP simulation, all the glycans, NGlyc and GPI, showed only a few interactions with the protein core of PrP. The H-bond analysis in Table III shows that throughout the simulation fewer than two hydrogen bonds on average occur between each N-linked glycan and the side chains of the protein. With an average of 1.4 H bonds, the GPI anchor has even less contact with the protein side chains. For all glycans in the model, most H bonds occur between the glycan and the solvent, and within each glycan. Interaction between the glycans was observed only for $NGlyc^{181}$ and $NGlyc^{197}$, with an average of 2.6 H bonds. One consequence of the weak direct interactions between glycans and protein is that there are few differences in the solvent accessibility of the protein side chains between the *Hu*PrP and glyc-*Hu*PrP models (see Figure 6). For a few residues, such as $Phe^{198}$ and $Thr^{199}$ in Turn-D and $Ile^{184}$ in Helix-B, the solvent accessibility is changed to totally buried. For other residues, such as $Asp^{178}$, $Lys^{185}$, $Thr^{192}$, $Thr^{193}$, and $Lys^{194}$ in Helix-B, the solvent accessibility is changed to less frequently exposed. Thus, the glycans restrict direct access to the protein only in a few places on the surface.

**Table III.** Average number of H bonds[a] throughout the simulation of the *Hu*PrP model with and without the oligosaccharides (*Hu*PrP and glyc-*Hu*PrP, respectively), the free NGlyc and GPI models in water (solv-NGlyc and solv-GPI) and the GPI model attached to a model membrane with choline (cho-GPI) or ethanolamine (eap-GPI) as the head group of the membrane monomer

| | | *Hu*PrP$^{90-231}$ | | NGlyc | | | | |
|---|---|---|---|---|---|---|---|---|
| Model | | Bb | Sc | Asn$^{181}$ | Asn$^{197}$ | GPI | Memb | Wat |
| *Hu*PrP | Bb | 202.7 | 40.6 | | | | | 186.0 |
| | Sc | | 48.6 | | | | | 272.2 |
| glyc-*Hu*PrP | Bb | 212.3 | 37.1 | 0.7 | 0.1 | 0.3 | | 177.0 |
| | Sc | | 42.8 | 1.9 | 1.8 | 1.4 | | 270.6 |
| | Asn$^{181}$ | | | 98.3 | 2.6 | 0.0 | | 172.9 |
| | Asn$^{197}$ | | | | 83.3 | 0.6 | | 191.6 |
| | GPI | | | | | 35.4 | | 92.1 |
| solv-NGlyc | NGlyc | | | 89.8 | | | | 195.8 |
| solv-GPI | GPI | | | | | 33.3 | | 76.7 |
| cho-GPI | GPI | | | | | 34.9 | 5.5 | 76.7 |
| eap-GPI | GPI | | | | | 34.5 | 9.2 | 78.7 |

[a]Analysis of the H bonds is split into protein backbone (Bb) and side chain (Sc) atoms, GPI anchor (GPI), *N*-linked glycan (NGlyc), membrane (Memb), and Water (Wat).

**Table IV.** Comparison between simulations of the GPI anchor and NMR experiments of similar GPI structures, showing corresponding NOE constraints from the NMR experiments I (Homans *et al.*, 1989) and II (Weller *et al.*, 1994), and average distances from the simulations

| | NOE-constraints (Å) | | Average distance in simulations (Å) | | | |
|---|---|---|---|---|---|---|
| | I [a] | II [b] | glyc-*Hu*PrP | solv-GPI | cho-GPI | eap-GPI |
| *m*Ino$^{II}$-H6 ↔ GlcN$^{III}$-H1 | 2.6 | 1.8–3.3 | 2.6 | 2.6 | 3.7 | 3.6 |
| GlcN$^{III}$-H4 ↔ Man$^{IV}$-H1 | 2.4 | 1.8–2.7 | 2.5 | 2.9 | 6.2 | 5.8 |
| Man$^{IV}$-H3 ↔ Man$^{V}$-H1 | | 1.8–2.7 | 6.8 | 6.8 | 6.2 | 6.7 |
| Man$^{IV}$-H2 ↔ Man$^{V}$-H5 | | 1.8–2.7 | 6.5 | 6.8 | 7.4 | 6.5 |
| Man$^{V}$-H1 ↔ Man$^{VI}$-H5 | 2.5 | | 3.2 | 2.8 | 5.2 | 2.9 |
| Man$^{V}$-H2 ↔ Man$^{VI}$-H1 | 2.3 | | 2.5 | 2.4 | 3.3 | 2.4 |

[a](*m*Ino$^{II}$-GlcN$^{III}$-Man$^{IV}$(-Gal-Gal…)-Man$^{V}$-Man$^{VI}$-$PO_2{}^{VII}$-Ea$^{VIII}$)
[b](*m*Ino$^{II}$-GlcN$^{III}$-Man$^{IV}$-Man$^{V}$(-$PO_2$-Glc)-Gal-Gal…).

But a weaker restriction on the accessibility can be seen in cases where only one water molecule is between the glycan and the protein. Although analysis of the distances between the glycan and protein shows only three direct interactions, considering a distance which would accommodate just one water molecule (distance < 6.5 Å) indicates that NGlyc$^{181}$ covers several residues in Helix-B and some in the turn before Strand-A, while NGlyc$^{197}$ covers nearly all the residues of Turn-D and some at the beginning of Helix-C. The glycan residues involved in this steric cover of the protein include the first few residues next to the linkage site to the protein, namely Man$^{IV}$-GlcNAc$^{III}$-(Fuc$^{II}$-)-GlcNAc$^{I}$-Asn$^{181/197}$. In addition to these core glycans residue, one of the SiaLe$^{x}$ groups, NeuNAc$^{XI}$-Gal$^{X}$-(Fuc$^{IX}$-)GlcNAc$^{VIII}$, of both NGlyc chains is in direct or water-bridged contact with the protein. While this shielding of PrP by the glycans might be "weak" if it were neutral, analysis of the electrostatic potential of the glycan cover shows a different picture. As both N-linked glycans have a net charge of –3 e.u., a negative electrostatic potential covers all the surface of Helix-B and Helix-C and a small part of Helix-A (see Figure 7).

The GPI anchor, on the other hand, covers only the surface of the last three residues of *Hu*PrP, and makes no direct contact with the protein. This cover involves only the first 2–3 GPI residues next to the linkage to the protein, i.e., Ser$^{230}$-Ea$^{VIII}$-$PO_2{}^{VII}$-(Man$^{X}$-)Man$^{VI}$. The GPI glycan occupies the space around the C-terminal end of Helix-C opposite the two N-linked glycans, and, as it has several negatively charged residues, it extends the negative electrostatic potential to the end of Helix-C.

### *GPI anchor in membrane*

To investigate a possible orientation and, especially, a possible distance of PrP with respect to the membrane, additional simulations were carried out involving a monolayer membrane with an embedded GPI anchor. For the membrane two different models were used, one with ethanolamine (eap-GPI) and one with choline (cho-GPI) as the membrane-head group. Both simulations showed the GPI-anchor glycan to be as

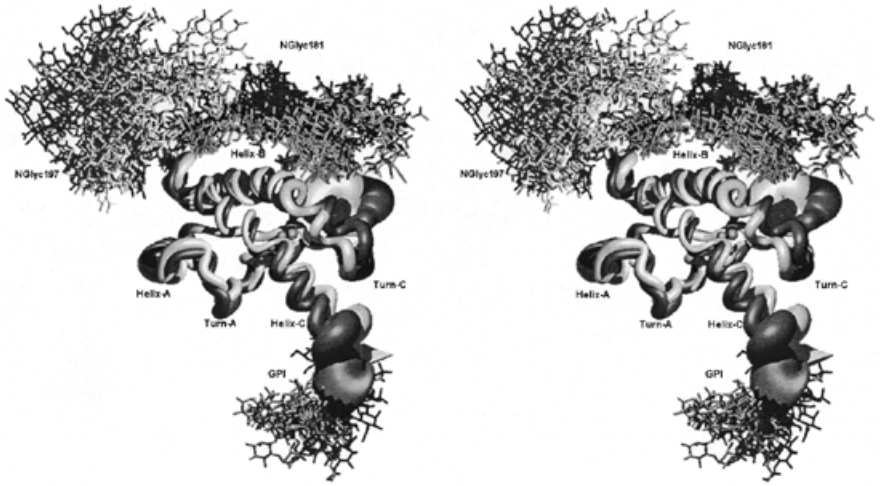


**Fig. 4.** Stereoview of the average structure of *Hu*PrP (black) and glyc-*Hu*PrP (gray) from the simulations. The protein structure, including *Hu*PrP from $Lys^{104}$ to $Ser^{230}$ only, is shown as a coil of the Cα trace, where the thickness of the coil represents the fluctuations of the Cα atoms. The thicker the coil the more flexible the structure is during the simulation. Also shown is the disulfide bridge ($Cys^{179}$-$Cys^{214}$). The N-glycans, $NGlyc^{181}$ and $NGlyc^{197}$, and the GPI anchor are shown as ball-and-stick representations for snapshots every 100 ps. The picture was generated using MOLMOL (Koradi *et al.*, 1996) and POVRAY (http://www.povray.org).

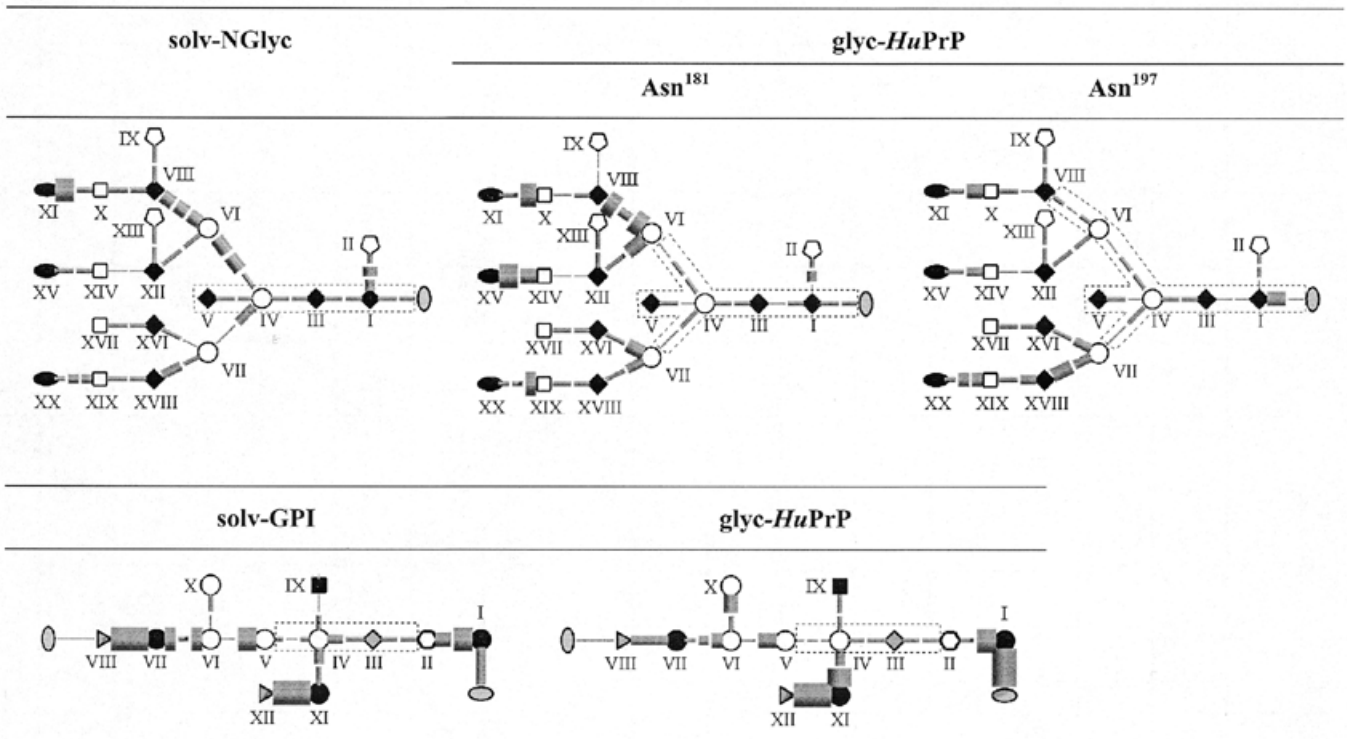


**Fig. 5.** SD of the backbone and glycosidic linkage torsion angles (ϕ and ψ, and ω in case of a 1–6 linkage) of the NGlyc and GPI models for MD simulations of glyc-*Hu*PrP and of the solvated glycans (solv-NGlyc and solv-GPI), shown as cylinders between the residue symbols (see Figure 1 for description of symbols), where the radius of the cylinder indicates the magnitude of the SD. The radii are grouped into ranges of SD: <5°, <10°, <25°, <35°, and <50°. Dotted boxes identify the core of the glycans with reduced flexibility.

flexible as in the simulations of the free GPI glycan in solution or the GPI glycan in the glyc-*Hu*PrP model. The average SD values of the linkage torsion angles are 31.2° and 27.7° (Table I) for the cho-GPI and the eap-GPI simulations, respectively, values similar to the other simulations. In both simulations, the GPI-anchor glycan has reduced flexibility in the first residues from the membrane linkage, with a unique conformation for the membrane-$PO_2^I$-*m*$Ino^{II}$-$GlcN^{III}$-$Man^{IV}$ residues (see Figure 8; compare with Figure 5), but with an average distance between *m*$Ino^{II}$-H6↔$GlcN^{III}$-H1 similar to the other simulations and

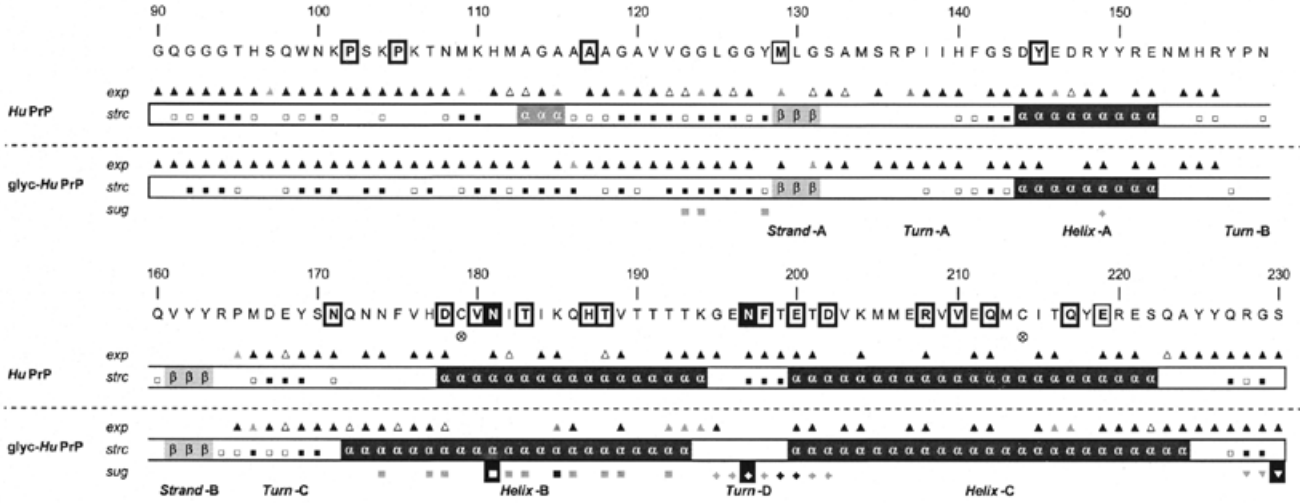


**Fig. 6.** Amino acid sequence of the *Hu*PrP$^{90-231}$ model used for the *Hu*PrP and glyc-*Hu*PrP simulations. Mutation sites which are associated with disease in humans are boxed (Ironside, 1998; Zuegg and Gready, 1999). A cross-hatched circle identifies the two cysteines in the disulfide bridge, and N with black background shows the two glycosylation sites. The solvent exposure (*exp*) of the amino acids for both simulations with and without the oligosaccharides is shown as: solid triangles, >75%, gray triangles, >50%, and open triangles, > 25% of the simulation time exposed. The structural information (*strc*) includes secondary structure present for more than 50% of the simulation time (α for α-helices, β for β-sheets), and flexibility of the backbone as SD of the backbone torsion angles: solid squares, >35° open squares, >25°. The distance of the oligosaccharides from the protein (*sug*) is shown for the three sugars separately: inverted solid triangles, GPI; solid squares, NGlyc$^{181}$, solid triangles, NGlyc$^{197}$, with gray indicating a distance < 6.5 Å (space for one water molecule), black indicating a distance < 3.5 Å (H-bond distance), and inverse denoting a distance < 2 Å (covalent bond).

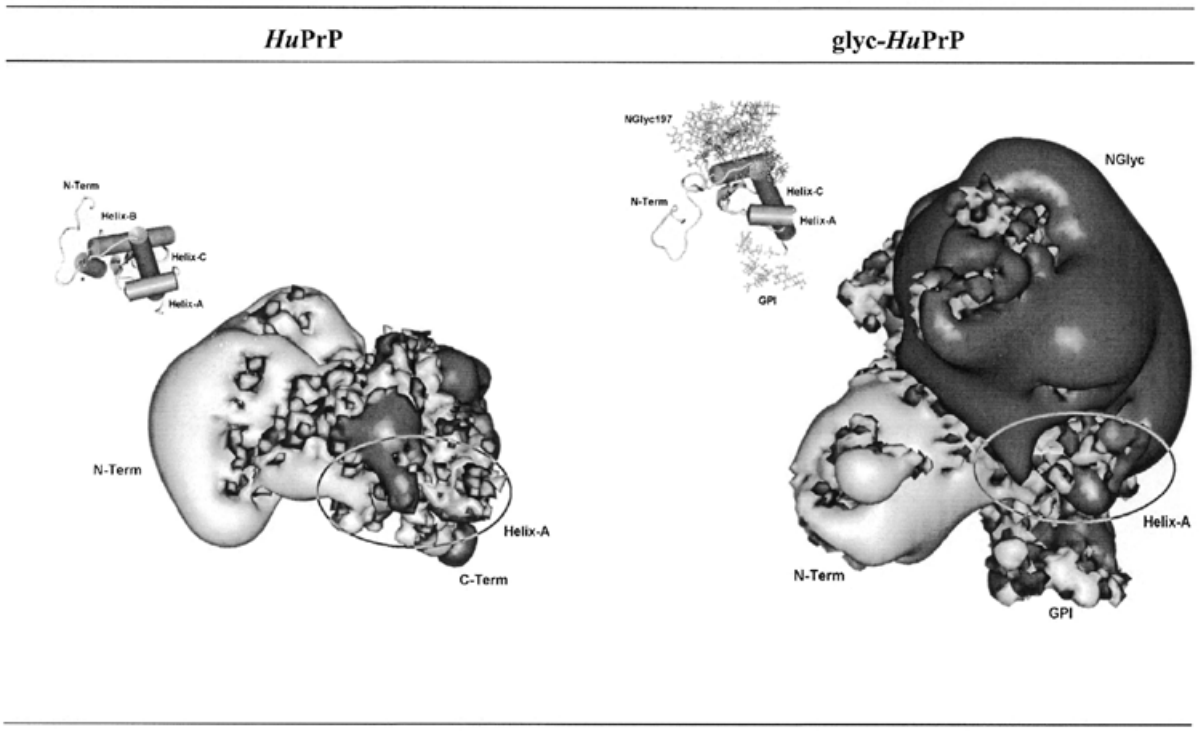


**Fig. 7.** Electrostatic potentials of *Hu*PrP and glyc-*Hu*PrP using structures at 1 ns simulation time. The electrostatic potential was calculated with DELPHI (Gilson and Honig, 1987) and displayed as contour surfaces at –2.0 kT/e (black) and 2.0 kT/e (gray). Both structures, shown in the small insert in secondary structure ribbon representation, are aligned in the same orientation. The circled area on the electrostatic contour surface identifies the surface area of Helix-A. The initial α-helix (*) in the hydrophobic region of the N-terminal part forms only during the *Hu*PrP simulation.

NMR experiments (see Table IV). The GlcN$^{III}$-Man$^{IV}$ linkage, on the other hand, shows a different conformation compared with the other simulations or NMR experiments. For both simulations, the remaining part of the GPI-anchor glycan has

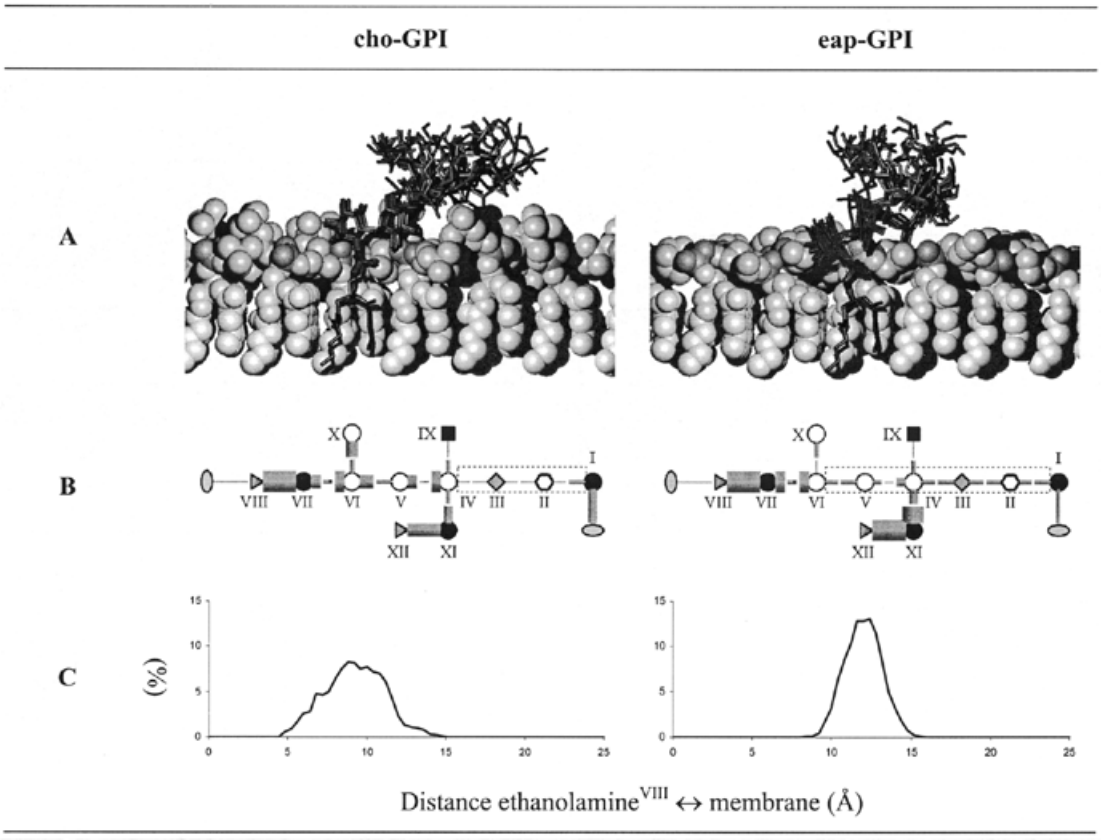


**Fig. 8.** Analysis of the MD simulations of the GPI anchor model attached to a membrane with choline (cho-GPI) or ethanolamine (eap-GPI) as membrane-head groups (**A**) Overlaid structures of the GPI model in all its different conformational clusters shown in stick model form, with the membrane shown in CPK representation. The picture was generated using MOLMOL (Koradi *et al.*, 1996) and POVRAY (http://www.povray.org). (**B**) SD of the backbone (Ea and $PO_2$ residues) and glycosidic-linkage torsion angles of the GPI model for both simulations, shown as cylinder between the residue symbols (see Figure 1 for description of symbols), where the radius of the cylinder indicates the magnitude of the SD. The radii are grouped into ranges of SD: <5°, <10°, <25°, <35° and <50°. Dotted boxes identify the core of the glycans with reduced flexibility. (**C**) Distribution of the minimum distance between the heavy atoms of the $Ea^{VIII}$ group, which would be linked to the protein, and the membrane.

high flexibility, especially in the -$PO_2^{VII}$-$Ea^{VIII}$ part which is linked to PrP in the glyc-*Hu*PrP model. The main difference between the two models is the distance of this ethanolamine group from the surface of the membrane. For the cho-GPI model, the distance ranges from 5.5 to 13.0 Å with an average of 8.8 Å, whereas for the eap-GPI model it ranges from 9.5 to 14.8 Å with an average of 12.3 Å. All simulations were carried out by fixing the position of the fatty acids, including that to which the GPI glycan is attached.

*Orientation of PrP with respect to the membrane*

To find a possible orientation of *Hu*PrP with respect to the membrane, we tried to combine directly the structures of the glyc-*Hu*PrP simulation with the structures of the two membrane simulations, cho-GPI and eap-GPI, by aligning only the GPI anchor. But, unfortunately, all resulting conformations had part of the *Hu*PrP structure overlapping the membrane. Therefore, models were generated by taking the GPI-anchor core structure, $Man^{V}$-$Man^{IV}$-$GlcN^{III}$-*m*$Ino^{II}$-$PO_2^{I}$-membrane from one of the membrane simulations, in this case from cho-GPI, and the remaining part of the GPI anchor from the glyc-*Hu*PrP simulation. We then varied the torsion angles of the $Ser^{230}$-$Ea^{VIII}$-$PO_2^{VII}$ group which links to *Hu*PrP, in such a way as to get structures with reasonable properties, e.g., no clashes between *Hu*PrP and the membrane. The first conformation we were able to generate was a structure in which the GPI anchor had approximately the same orientation with respect to PrP as in the glyc-*Hu*PrP simulation (A in Figure 9). In this conformation, the PrP is *lying down* on the membrane with its Helix-A close to the membrane and the two NGlyc chains facing in the opposite direction. The N-terminal part of *Hu*PrP is, thus, close to the membrane as well. As the N-terminal region of PrP has an overall positive electrostatic potential (see Figure 7) this might result in an unfavorable orientation.

The second type of conformation we generated is based on several concepts: that GPI-anchored proteins have a tendency to form multimers on the surface of membranes (Ferguson, 1992; Vaughan, 1996; Maxfield and Mayor, 1997; Friedrichson and Kurzchalia, 1998; Varma and Mayor, 1998); that a dimer of PrP has been reported (Priola *et al.*, 1995); that the first step in the propagation of $PrP^{Sc}$ is suggested to be complex formation between $PrP^{Sc}$ and $PrP^{C}$ (Prusiner, 1991) and that the primary binding site for such a complex is suggested to be the region $PrP^{119–141}$ (Warwicker, 1997; Horiuchi and Caughey, 1999); and that Helix-A may also act as a hydrophilic seed for such dimerization (Morrissey and Shakhnovich, 1999). The

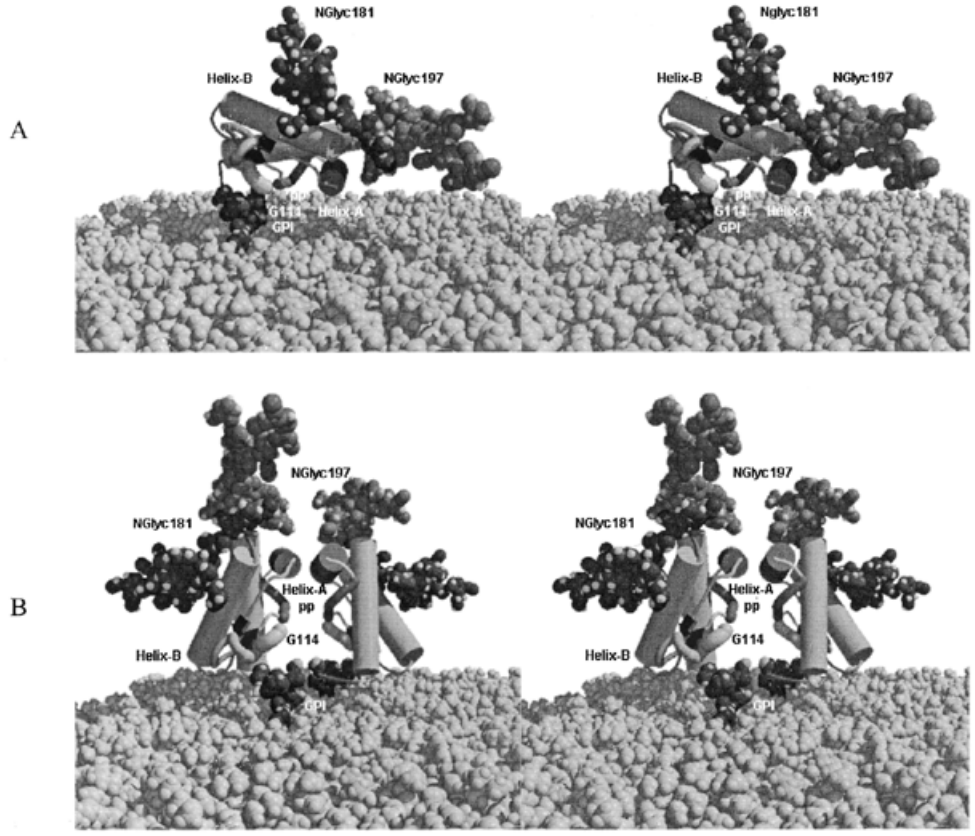


**Fig. 9.** Stereo representation of two possible orientations of *Hu*PrP with respect to the membrane. (**A**) shows the monomeric *lying-down* model in which Helix-A is in close contact with the polar surface of the membrane. (**B**) shows the dimeric *standing* model with Helix-A and the C-terminal part of the $PrP^{Sc}$-$PrP^{C}$ binding region, *Hu*$PrP^{135–141}$ (pp; Horiuchi and Caughey, 1999) forming the interaction between the two monomers.

resulting conformation, shown in Figure 9B, has PrP *standing* on the membrane, with the GPI glycan forming an extension to Helix-C and with the two NGlyc chains even further away from the membrane. Figure 9B shows a possible dimer in which the two Helix-A's are in antiparallel orientation. This antiparallel aggregation would allow the formation of four salt bridges between the two helices (Morrissey and Shakhnovich, 1999). In addition, the two C-terminal regions of the $PrP^{Sc}$-$PrP^{C}$ binding region (Horiuchi and Caughey, 1999), $PrP^{135–141}$ (see pp in Figure 9B), are also in close proximity in an anti-parallel orientation. A similar region was used as the major interaction site between the monomers in the proposed dimer model of Warwicker (1997). The N-terminal parts of the *Hu*PrPs are oriented in opposite directions, and are further away from the membrane than in the *lying-down* conformation. The NGlyc chains would not interfere with Helix-A aggregation, but would create a negative electrostatic potential all around the dimer, with two positive potentials from the N-terminal parts of PrP oriented parallel to the membrane but in opposite directions.

## Discussion

Mammalian PrP contains two consensus sites for N-linked glycosylation, $Asn^{181}$ and $Asn^{197}$ in *Hu*PrP. Deactivating the N-glycosylation site at $Asn^{180}$ (*Mo*PrP) by mutating $Thr^{182}$→Ala, led to intracellular accumulation of PrP, whereas deactivating the N-glycosylation site at $Asn^{196}$ by a $Thr^{198}$→Ala mutation, showed no intracellular accumulation, but reduced delivery of PrP to the plasma membrane (Rogers *et al.*, 1990; Lehmann and Harris, 1997). Both mutations showed properties of a $PrP^{Sc}$-state form (Lehmann and Harris, 1997), but only one of the two mutations, $Thr^{183}$→Ala in *Hu*PrP, is actually known to be disease-related in humans (Ironside, 1998). Apart from being important for cell trafficking, the N-glycosylations have been suggested to have an influence on the folding process and structural stability of PrP (Harris, 1999). Studies with the $Asp^{178}$→Asn mutation, which is also associated with CJD and FFI in humans (Ironside, 1998) and is close to the $Asn^{181}$ glycosylation site, suggested that the instability of the mutant PrP is partially corrected by N-glycosylation (Petersen *et al.*, 1996). This stabilization is further suggested to be influenced by the amino acid at position 129 (Met or Val). It has been suggested that PrP has an intrinsic tendency to acquire $PrP^{Sc}$-like properties and protease resistance, and that the N-glycan chains might protect it against these changes (Lehmann and Harris, 1997). This suggestion is based on experiments that indicate correct folding of PrP is essential for correct processing and biosynthetic transport of the protein: for example eliminating the disulfide bridge (Capellari *et al.*, 1999; Ma and Lindquist, 1999; Yanai *et al.*, 1999) resulted in PrP being trapped in the

endoplasmic reticulum (ER) where it accumulated in a $PrP^{Sc}$-like form (Daude *et al.*, 1997; Hedge *et al.*, 1998). Glycosylation is able to protect PrP against incorrect folding in the ER, but is not necessarily required for biosynthetic transport (Lehmann and Harris, 1997). For example, analysis of $PrP^{Sc}$ revealed different glycosylation forms ranging from di-, to mono- to non-glycosylated PrP (Caughey *et al.*, 1989). Even though different prion strains sometimes display distinctive glycosylation patterns (Harris, 1999), no straightforward relationship could be identified between the different glycosylations and the natural cycling of PrP between cell surface and endosomes, or the formation of $PrP^{Sc}$ in late endosomes.

Detailed chemical analysis of the carbohydrate chains of $PrP^{Sc}$ purified from scrapie-infected hamster brain showed that both N-glycosylation sites of PrP are occupied, and that a mixture of bi-, tri-, and tetra-antennary complex-type oligosaccharide chains is present, with about 70% of the terminal galactose residues linked to sialic acid (Endo *et al.*, 1989). More detailed analysis of $PrP^{Sc}$ from scrapie-infected mouse showed similar oligosaccharide structures as for hamster PrP (Rudd *et al.*, 1999a; Stimson *et al.*, 1999). In addition, the analysis revealed that the termini of the oligosaccharides consist of $Lewis^x$ ($Le^x$) and sialyl $Lewis^x$ groups ($SiaLe^x$), Galβ(1–4)(Fucα(1–3))GlcNAc and NeuNAcα(2–3)Galβ(1–4)(Fucα(1–3))GlcNAc, respectively. The structures of all these different oligosaccharides, 60 altogether, seem to derive from one tetra-antennary oligosaccharide complex by partial degradation. Both N-glycosylation sites are found to have the same oligosaccharide complex, although with slightly different degradation stages. Even though all detailed structural studies of the oligosaccharides of PrP have been made on $PrP^{Sc}$, the cellular form $PrP^{C}$ is suggested to have a similar type of oligosaccharide composition (Haraguchi *et al.*, 1989). A recent, more detailed study indicated that $PrP^{C}$ and $PrP^{Sc}$ contain the same set of oligosaccharides, but with different relative proportions of individual glycans (Rudd *et al.*, 1999a).

In this work we investigated the possible influence of the N-linked oligosaccharides and the GPI anchor on the protein structure of human PrP (*Hu*PrP). To achieve this, we compared the trajectories from a molecular dynamics (MD) simulation of *Hu*PrP with all oligosaccharides (glyc-*Hu*PrP) with those from a simulation of *Hu*PrP without any of the glycans (*Hu*PrP). Previous MD simulations (Zuegg and Gready, 1999) showed that the structures of a homology model of *Hu*PrP and the NMR structure of *Sh*PrP are highly sensitive to the electrostatic environment, and that only correct treatment of the long-range electrostatic interactions resulted in a stable structure. As both N-glycans can carry up to three negatively charged $SiaLe^x$ groups, which would change the electrostatic environment of *Hu*PrP significantly, investigating their effect on the protein structure appeared necessary. For the fully glycosylated *Hu*PrP model, a N-glycan model was generated, which can be considered as the glycan from which all the oligosaccharides found experimentally (Endo *et al.*, 1989; Rudd *et al.*, 1999a; Stimson *et al.*, 1999) could be derived by partial degradation. However, as the exact branching structure could not be determined in the experiments the model has some uncertainties, for example the distribution of the $SiaLe^x$ groups among the branches. Similarly, the GPI-anchor model used also has some uncertainty, as experiments could neither identify the type of glycosidic linkage nor the anomeric type in one branch (Stahl *et al.*, 1987, 1992; Baldwin *et al.*, 1993).

In the MD simulation of the glyc-*Hu*PrP model, both C-terminal α-helices, Helix-B and Helix-C, not only have increased length compared with the simulation of non-glycosylated *Hu*PrP, but also the split in Helix-C observed in the *Hu*PrP simulation does not occur. In addition, residues in Turn-D, between Helix-B and C, showed reduced variation in the backbone torsion angles. On the other hand, residues in Turn-C, between Strand-B and Helix-B, showed increased variation of the backbone torsion angles during the simulation, as did the residues in the N-terminal part, $PrP^{90–126}$. Taken together, the results suggest that most of the *structured* part of the protein, $HuPrP^{127–227}$, experiences a stabilizing effect from addition of the glycans. The perturbation to Turn-C by the presence of the glycan is not associated with any direct interaction between Turn-C and $NGlyc^{181}$ or with the GPI anchor. NMR experiments of $MoPrP^{121–231}$ (Billeter *et al.*, 1997), $ShPrP^{90–231}$ (James *et al.*, 1997), and *Hu*PrP (Hosszu *et al.*, 1999) show variations in the lengths of all three α-helices, similar to the differences found between our glycosylated and nonglycosylated *Hu*PrP models. Although the C-terminal part of PrP forms a defined structure very quickly (Wildegger *et al.*, 1999), the differences found in the NMR experiments may be attributed to the lack of glycans. As absence of the glycans results in higher flexibility of the protein backbone, different sequences might adjust to this potential instability differently, some in Turn-D and some in Helix-C. Our simulation of the glycosylated *Hu*PrP model suggests that both N-glycans are able to stabilize PrP in these regions.

The N-terminal part of *Hu*PrP, $HuPrP^{90–127}$, changes its dynamical behavior to more flexible on glycosylation. However, this may be due to the fact that its starting conformation was randomly chosen as NMR experiments show it is disordered and, thus no structural data are available. Hence, using a different starting conformation might result in different structural and dynamical behavior of the N-terminal part. Despite these uncertainties, the simulations suggest that glycans have some structural influence on the N-terminal part of *Hu*PrP, especially on the residues immediately before the first strand, $HuPrP^{120–130}$, which are close to $NGlyc^{181}$. It is possible that this part would form a defined structure under the influence of the glycans, but unfortunately the simulation time of ~2 ns is far too short to see development of any significant secondary structure.

Interestingly, the influence of the glycans on the protein appears not to be due to specific direct interactions, such as H bonds or salt bridges. Indeed, each glycan has only one to two H-bond interactions with the protein. The influence of the glycans seems to be more indirect, by reducing the mobility of the surrounding water molecules. Throughout the simulation, some parts of the glycans in both NGlyc chains are not more then one water molecule away from the protein. Thus, both N-glycans together cover all residues in Turn-D and all surface-facing residues of Helix-B. This includes $Lys^{194}$, which is reported to be a cleavage point for trypsin only when the glycan at the $Asn^{197}$ site is small (Stimson *et al.*, 1999). In addition, $NGlyc^{197}$ covers one residue in Helix-A and $NGlyc^{181}$ some residues just before the first strand. The extent of the area covered by the N-glycans depends, of course, on their conformations. The current simulations can be considered only as an estimate for the nature and extent of the glycan cover, due to uncertainties in the glycan models used and the fact that a full investigation

of the conformational space of the glycans would require simulations 100 times longer (Peters and Pinto, 1996). However, as the main feature of the N-glycan cover is its negative electrostatic potential, produced by the charged $SiaLe^x$ groups, its extent is less sensitive to conformational details of the glycans. The negative electrostatic field extends over the whole surface of Helix-B and Helix-C onto the opposite side of PrP to Helix-A. Even though the N-glycans do not sterically cover Helix-C, the negative field extends to the C-terminal end of Helix-C because of negatively charged residues on the surface of Helix-C and because of the $PO_2$ group in the GPI anchor. The field has a positive counterpart at the N-terminal part of the *Hu*PrP model, which has several positively charged residues. The orientation of the dipole moment depends entirely on the position of the N-terminal part, which in all simulations and NMR experiments shows no defined structure. In between the two dominant fields is Helix-A, which has a quite unusual nature. Helix-A, $PrP^{144–152}$, with an amino acid sequence of DYEDRYYRE, is entirely hydrophilic and is stabilized by the salt bridges $Glu^{146}\leftrightarrow Arg^{208}$, between Helix-A and Turn-D, and $Arg^{156}\leftrightarrow Glu^{196}$, between the neighboring Turn-B and Turn-D. Interestingly, $Arg^{208}$ is a residue whose mutation into His is known to be associated with inherited forms of human disease (Ironside, 1998). The charged surface residues of Helix-A makes it a good candidate for aggregation in either a parallel or anti parallel orientation, forming in each case two salt bridges (Morrissey and Shakhnovich, 1999). As Helix-A is not covered by either of the dominant electrostatic fields, it is, therefore, electrostatically accessible. An antiparallel aggregation would not disrupt its structure, and would lead to the *Hu*PrP dimer as shown in Figure 9B, with an extended cover by the N-glycans on top and on the side and with the N-terminal parts sticking out in opposite directions from the middle. A PrP dimer seems to occur naturally (Priola *et al.*, 1995) or, at least, be the starting point for the conversion from $PrP^C$ to $PrP^{Sc}$ (Prusiner, 1991; Warwicker, 1997). By contrast, a parallel aggregation of Helix-A would disrupt the helical structure and lead to β-nucleation, which has been suggested to form the mechanism for the conversion of $PrP^C$ to $PrP^{Sc}$ (Morrissey and Shakhnovich, 1999). Interestingly, a mutation of $Arg^{208}$ would disrupt the salt bridge between Helix-A and Turn-D and might, thereby, facilitate the transformation of Helix-A into β-sheet conformation, necessary for the parallel aggregation. On the other hand, our model suggests that the N-glycans are not favorable for such an orientation, even though such aggregation could include major rearrangements in the N-terminal part of the *structured* portion of PrP, and, thus, would lead to different locations and relative orientations of the residues of the former Helix-A region, such as opposite Helix-B and Helix-C as in a proposed model of $PrP^{Sc}$ (Huang *et al.*, 1996). However, in addition to inferences from our model, experiments showed that binding of antibody specific for the Helix-A region is not able to inhibit the first step in the formation and aggregation of $PrP^{Sc}$, namely the binding of $PrP^{Sc}$ to $PrP^C$ (Horiuchi and Caughey, 1999).

The antibody-binding experiments also showed that antibody specific for the region $PrP^{218–231}$ is able to inhibit the binding of $PrP^{Sc}$ to $PrP^C$ (Horiuchi and Caughey, 1999). This region is in the vicinity of the *protein X* binding region (Telling *et al.*, 1995; $Glu^{168}$, $Gln^{172}$, $Ile^{215}$, and $Glu^{219}$), where *protein X* is suggested to play a role during $PrP^{Sc}$ propagation (Kaneko *et al.*, 1997a). Even though this region, involving Turn-C and the end of Helix-C, is not entirely covered by the N-glycans the proximity of the negative electrostatic potential would not favor an aggregation in this region. As both N-glycans and the GPI anchor do not influence the formation of the $PrP^{Sc}$-$PrP^C$ complex (Kaneko *et al.*, 1997b) and PrP lacking Turn-C is still able to generate a $PrP^{Sc}$-like form (Muramoto *et al.*, 1996), the region around Strand-A, $PrP^{119–138}$, has been suggested to form the potential binding site in $PrP^{Sc}$-$PrP^C$ complex formation (Horiuchi and Caughey, 1999). In addition, this region includes some of the residues important for the species barrier for disease transmission (Kocisko *et al.*, 1995; Schätzl *et al.*, 1995), and was used as the primary binding site for a dimer model (Warwicker, 1997). In our solvated model glyc-*Hu*PrP (Figure 4), this region is not influenced by the oligosaccharides and is exposed to the solvent. The monomer model of the membrane-bound *Hu*PrP (Figure 9A) shows this region is close to the membrane. On the other hand, the dimer model (Figure 9B) has part of this proposed $PrP^{Sc}$-$PrP^C$ binding region, $PrP^{135–141}$ next to each other. The earlier proposed dimer model (Warwicker, 1997) used the $PrP^{130–136}$ region as the primary binding site, but this resulted in a different orientation, in which both C-terminal ends were pointing in opposite directions, thus making it impossible for both monomers to be bound to the membrane by GPI anchors. Our dimer model can be seen as a possible model not only for a reported naturally occurring dimer (Priola *et al.*, 1995), but also as a possible dimer starting point in $PrP^{Sc}$ propagation. The monomer model shows the N-terminal part of PrP closer to the membrane, more in agreement with experiments suggesting that this part makes strong interactions with the membrane (Morillas *et al.*, 1999), but due to the uncertainty of the structure and its high flexibility, an orientation of this N-terminal part towards the membrane is not excluded in the dimer model.

The mutation experiments which deactivated each N-glycosylation site (Lehmann and Harris, 1997), showed that the $Asn^{181}$ site seems to be associated more with a cell-trafficking role, whereas the $Asn^{197}$ site seems to stabilize the PrP structure. Structures from the glyc-*Hu*PrP simulation show $NGlyc^{181}$ affecting an area which already has a stable secondary structure, whereas $NGlyc^{197}$ affects an otherwise more flexible area of a turn by reducing its flexibility. This is consistent with $Asn^{181}$ glycosylation having a more functional role. A similar suggestion has been made in comparing PrP with the PrP-like protein doppel (Dpl), where only the site analogous to $Asn^{181}$ is conserved in the Dpl sequence (Asn111; Moore *et al.*, 1999). Note, however, that $NGlyc^{181}$ contributes more to the negative electrostatic potential covering of *Hu*PrP, as $NGlyc^{197}$ is more solvent exposed. The second N-glycosylation site of Dpl at $Asn^{99}$ would be in Turn-C which, assuming a similar 3-D structure, would result in an N-glycan oriented on the same side of the protein as $Asn^{111}$ but closer to the C-terminal part of the protein. In addition, this site is closer to $Asn^{111}$ than $Asn^{191}$ is to $Asn^{181}$ in PrP, thus restricting the available space for oligosaccharides, and suggesting that the N-glycans of Dpl might be a different size compared with the PrP N-glycans, and cover Helices B and C at the C-terminal part of the protein more than in the Turn-D region as in PrP.

The model for the N-glycans used in this work represents the largest and the most charged glycan possible. In addition, both

N-glycosylation sites were considered to be occupied by the same glycan. Partial degradation of the N-glycans would, of course, change their properties, especially cleavage of the charged NeuNAc residues would reduce the negative electrostatic potential. Detailed analysis of the N-glycans of PrP showed substantial heterogeneity in their structure (Endo *et al.*, 1989; Rudd *et al.*, 1999a; Stimson *et al.*, 1999). It has also been reported that $PrP^{Sc}$ strains, encoding distinct disease phenotypes, are associated with different patterns of glycosylation (Collinge *et al.*, 1996; Mastrianni *et al.*, 1999; Somerville, 1999). However, our work showed that even the most charged N-glycans do not have a major influence on the conformational structure of *Hu*PrP, and that most of the important parts of $PrP^{C}$ with respect to proposed mechanism for $PrP^{Sc}$ formation (N-terminal part, Strand-A, Turn-A, and Turn-C), are accessible even with the largest possible N-glycans. Recent experiments showed a different glycosylation pattern between $PrP^{C}$ and $PrP^{Sc}$, which correlated with differences in the activity of N-acetylglucosaminyltransferase III and suggested that some cells forming $PrP^{Sc}$ undergo changes that diminish the activity of an enzyme in the glycosylation pathway (Rudd *et al.*, 1999a). Also, different protein conformations can be attributed to different $PrP^{Sc}$ strains (Caughey *et al.*, 1989; Hill *et al.*, 1997; Safar *et al.*, 1998), with some conformational differences being correlated with concentrations of $Cu^{2+}$ and $Zn^{2+}$ ions (Wadsworth *et al.*, 1999). Taken together, these results suggest that the structure of $PrP^{Sc}$ is more variable than the $PrP^{C}$ structure, and that the structure of $PrP^{Sc}$ is more sensitive to particular aspects of the environment, such as the presence of metal ions or glycosylation, or the more general status of the $PrP^{Sc}$ forming cell.

The GPI anchor appears to have only a minor influence on the structure of *Hu*PrP, in contrast to the report for the Thy-1 protein (Barboni *et al.*, 1995). Its role seems to consist entirely in attaching PrP to the membrane. Simulations of the GPI anchor in a membrane showed that it keeps the protein at a distance between 9 and 13 Å from the membrane surface, depending on the type of membrane-head group. This distance is enough to maintain several water shells between the membrane surface and the protein and is, thus, enough to guarantee a high degree of freedom for the movement and orientation of PrP. This orientational freedom is assisted by the structurally flexible linkage group, ethanolamine, and by the C-terminal end of the protein which does not have any interactions with the rest of the model and is highly flexible.

In summary, it has been shown that the N-linked glycans do reduce the flexibility of the protein backbone in some parts of PrP, such as residues in the turn between Helix-B and Helix-C and within those helices, but perturb it in other parts to increase the flexibility, such as residues in the turn between Strand-B and Helix-B. But the main influence of the N-glycans appears to come from its negative charges, generating a negative electrostatic field which covers the whole surface of Helix-B and Helix-C. In addition, the simulations show that the GPI anchor has little influence on the structure of PrP. Its flexible structure guarantees a high degree of freedom for the orientation of PrP, but at the same time keeps the protein 9–13 Å above the membrane surface. A possible orientation of *Hu*PrP could be generated which takes into account the unique nature of Helix-A and the reported $PrP^{Sc}$-$PrP^{C}$ binding regions, allowing *Hu*PrP to form a homodimer on the membrane.

## Materials and methods

### *Force field parameter set*

All molecular dynamics simulations were carried out using the AMBER 5 package (Pearlman *et al.*, 1995; Case *et al.*, 1997) and the all-atom Amber94 force field (Cornell *et al.*, 1995). For the oligosaccharides, the Glycam93 force field (Woods *et al.*, 1995) was adapted to the Amber94 force field. The Glycam93 parameter set was originally generated by adding 3 atomtypes (anomeric carbon atom for each anomer and the glycosidic oxygen) to the standard protein Amber91 force field (Weiner *et al.*, 1986). In cases where the parameters in Glycam93 for the relevant tetrahedral carbon atom and the ethertype oxygen atom were the same as those in the Amber91 parameter set, the parameters were changed to the corresponding Amber94 parameter set values. These comprised all the van der Waals parameters and most of the dihedral parameters. For the other cases, which included mostly bond distance and bond angle parameters, the parameters were set to the original Glycam93 parameter set values. The main difference between Amber91 and Amber94 parameters is the absorption of the H-bond energy term into the van der Waals parameters and partial charges (Cornell *et al.*, 1995). Therefore, partial charges of all sugar residues have been recalculated in the same way as for the Amber94 parameter set, namely by fitting the electrostatic potential, calculated with the *ab initio* method HF/6–31G* using GAUSSIAN94 (Frisch *et al.*, 1994), with the RESP program (Cornell *et al.*, 1993). Default conformations for the sugar residues have been used, using the $^{1}C_{4}$ conformation for Fucα, the $^{2}C_{5}$ conformation for NeuNAcα and the $^{4}C_{1}$ conformation for all remaining sugars. In the same way, partial charges have been generated for the new non-sugar residues *myo*-inositol, ethanolamine, choline and diacylglycerol. Default bonding parameters for these residues have been used.

### *Model building for glyc-HuPrP*

The *Hu*PrP model was generated as described previously (Zuegg and Gready, 1999), and consists of a homology model of human $PrP^{90–230}$ based on the NMR structure of Syrian hamster PrP (James *et al.*, 1997). The *Hu*PrP model had its ionizable residues set to their solution ionization state at pH 7, as calculated with the program TITRA (Petersen *et al.*, 1997). The starting models for the N-linked glycan (NGlyc) and GPI-anchor (GPI) oligosaccharides were generated by assuming a $^{1}C_{4}$ conformation for Fucα, a $^{2}C_{5}$ conformation for NeuNAcα and a $^{4}C_{1}$ conformation for all remaining sugar residues, and changing only the glycosidic linkage torsion angles to produce a model with no steric clashes. Several minimization steps were required in the building process to obtain a low energy conformation of the models. The model oligosaccharides were attached to the *Hu*PrP model, one N-linked glycan model at each Nδ atom of $Asn^{181}$ and $Asn^{197}$, and one GPI model at the backbone C atom of $Ser^{230}$. The GPI model was terminated at the $PO_2^I$ group with a $CH_3$ group. The resulting model, glyc-*Hu*PrP, has 3376 atoms and a molecular mass of 25.3 kDa, compared with the *Hu*PrP model with 2180 atoms and a mass of 16.0 kDa. In order to use the particle mesh Ewald (PME) method (Darden *et al.*, 1993) for the calculation of long-range electrostatic interactions in the simulations, the system has to be neutralized. As in the previous work (Zuegg and Gready, 1999), this was achieved by adding $Na^{+}$ and $Cl^{-}$ ions to the

system. For the glyc-*Hu*PrP model, 20 $Na^+$ and 15 $Cl^-$ ions were added with the CION program in the AMBER 5 package, compared with 12 $Na^+$ and 13 $Cl^-$ ions added to the *Hu*PrP model. Both models were immersed in a rectangular box of pre-equilibrated TIP3 water molecules (Jorgensen *et al.*, 1983), of dimensions of $66 \times 63 \times 58$ Å, containing 5143 water molecules for the *Hu*PrP model, and $68 \times 86 \times 78$ Å with 10321 water molecules for the glyc-*Hu*PrP model.

*Model building for solvated glycans*

To analyze any structural and dynamical restrictions of the glycans due to the protein, simulations were carried out with free glycan models. The same NGlyc model as used as a starting model for glyc-*Hu*PrP was capped at the first $GlcNAc^1$ with a NH-CO-$CH_3$ group, neutralized by adding 3 $Na^+$ ions with the CION program, and immersed in a box of water (solv-NGlyc). Similarly, a solvated, free GPI-anchor glycan model, solv-GPI, was generated by replacing the protein backbone with a CO-$CH_3$ group on one side and the membrane glycerol with a $CH_3$ group on the other side. After adding one $Na^+$ ion to neutralize the model, the system was immersed in a box of water. Both solvated models were simulated with the same MD parameters as the *Hu*PrP and glyc-*Hu*PrP models.

*GPI anchor and membrane model*

For simulations of the GPI anchor attached to a membrane, two different models were generated differing only in the head group of the membrane monomer. The membrane was generated as a monolayer of a short $C_{5:0}$ fatty acid using 1,2-divalerianyl-phosphatidyl-ethanolamine (eap-GPI) or 1,2-divalerianyl-phosphatidyl-choline (cho-GPI) as the monomer. The GPI-anchor model was attached to the membrane by replacing one of the head groups with the GPI glycan. The GPI-anchor model was then covered by a cap of water molecules, containing 1244 and 1107 water molecules for eap-GPI and cho-GPI, respectively.

*MD simulations*

All MD simulations were performed using the SANDER module in the AMBER package. Systems were equilibrated by minimization and short constant pressure simulations as described in the previous work (Zuegg and Gready, 1999). In the simulations, Newton's equations of motion were integrated with a step size of 1 fs, with lengths of all bonds involving hydrogen atoms constrained using the SHAKE algorithm with a relative tolerance of $5 \times 10^{-6}$ Å. A pair-list to calculate non-bonded interactions was generated every 50 simulation steps. The temperature of the system was controlled to be 300 K using two independent Berendsen thermostats (Berendsen *et al.*, 1984), one for the solute and one for the solvent, and with coupling times $\tau_{Solute} = 0.5$ ps and $\tau_{Solvent} = 0.75$ ps.

For all models in a box of water, *Hu*PrP, glyc-*Hu*PrP, solv-Nglyc, and solv-GPI, the PME method was used to calculate the electrostatic interactions, using grid sizes which produce a grid spacing of ~1 Å. These simulations were carried out using periodic boundary conditions and constant volume, and removing the overall translational and rotational motion of the system every 100 time steps.

For the models with a water cap, cho-GPI and eap-GPI, no PME or periodic boundary conditions could be used. Instead, the electrostatic interactions were calculated by truncating the interaction at a distance of 8 Å, with the water cap being restrained to its cap-like form. In addition, the fatty acids of the membrane model were restrained to their starting positions, in order to maintain the shape of the monolayer.

*Analysis*

NMR experiments on $ShPrP^{90\text{-}231}$ revealed a highly flexible N-terminal part with only the C-terminal part having a defined secondary structure (James *et al.*, 1997). Therefore, all the root-mean-square deviation (RMSD) analysis of the structure was calculated not only for the complete model ($PrP^{90–230}$), but also for the *flexible* part ($PrP^{90–126}$) and the *structured* part ($PrP^{127–227}$) separately. Analysis of molecular trajectories was done with the program CARNAL in AMBER 5, including structural alignment and calculation of the RMSDs of the structures, and also torsion angle analysis. Analysis of the secondary structure was done with the DSSP program (Kabsch and Sander, 1983). Salt bridges were defined by the distance between the positively and negatively charged heavy atoms. For Arg residues, all three nitrogen atoms of the side chain, $N^{\varepsilon}$, $N^{\eta 1}$,$N^{\eta 2}$, were used. A salt bridge was deemed present if the distance between the two heavy atoms less the corresponding van der Waals radii was less than 1.5 Å. Calculation of the electrostatic potential was carried out with the DELPHI program (Gilson and Honig, 1987) in INSIGHTII-98 (1998, Molecular Simulations Inc., San Diego, CA), using default van der Waals radii and the same partial charges as in the simulation with AMBER. For model manipulation and visual analysis, INSIGHTII was used. The pictures were generated using MOLSCRIPT (Kraulis, 1991), RASTER3D (Merritt and Bacon, 1997), MOLMOL (Koradi *et al.*, 1996) and POVRAY (http://www.povray.org). The calculations and analysis were carried out on SGI Power-Challenge (SGI-PC) and Fujitsu VPP300 (VPP) supercomputers, and SGI Indigo2 and Octane workstations.

## Acknowledgments

We thank Dr. Thomas Huber for providing the optimized SANDER version of AMBER 5.0 for the VPP supercomputer and assisting on technical and scientific questions. We are grateful to the Australian National University Supercomputer Facility for providing computer time on the SGI and VPP supercomputers.

## Abbreviations

PrP, prion protein; *Hu*PrP, human prion protein; *Sh*PrP, Syrian hamster prion protein; *Mo*PrP, mouse prion protein; Dpl, doppel protein; CJD, Creutzfeld-Jacob disease; GSS, Gerstmann-Sträussler-Scheinker syndrome; FFI, fatal familiar insomnia; ER, endoplasmic reticulum; GPI, glycosyl phosphatidylinositol; Man, D-mannose; GlcNAc, N-acetyl D-glucosamine; GlcN, D-glucosamine; Gal, D-galactose; GalNAc, N-acetyl-D-galactosamine; NeuNAc, N-acetyl-D-neuraminic acid; Fuc, L-fucose; *m*Ino, *myo*-inositol; Ea, ethanolamine; $SiaLe^x$, sialyl $Lewis^x$, NeuNAcα(2–3)Galβ(1–4)(Fucα(1–3))GlcNAc; MD, molecular dynamics; PME; particle mesh Ewald; RMSD, root mean square deviation; SD, standard deviation.

## References


Agrawal,P.K., Jacquinet,J.C. and Krishna,N.R. (1999) NMR and molecular modeling studies on two glycopeptides from the carbohydrate-protein linkage region of connective tissue proteoglycans. *Glycobiology*, **9**, 669–677.

Arnold,J.E., Tipler,C., Laszlo,L., Hope,J., Landon,M. and Mayer,R.J. (1995) The abnormal isoform of the prion protein accumulates in late-endosome-like organelles in scrapie-infected mouse brain. *J. Pathol.*, **176**, 403–411.

Baldwin,M.A., Burlingame,A.L. and Prusiner,S.B. (1993) Mass spectrometric analysis of a GPI-anchored protein: the scrapie prion protein. *Trends Anal. Chem.*, **12**, 239–248.

Barboni,E., Rivero,B.P., George,A.J., Martin,S.R., Renoup,D.V., Hounsell,E.F., Barber,P.C. and Morris,R.J. (1995) The glycophosphatidylinositol anchor affects the conformation of Thy-1 protein. *J. Cell Sci.*, **108**, 487–497.

Berendsen,H.J.C., Postma,J.O.M., van Gunsteren,W.F., DiNola,A. and Haak,J.R. (1984) Molecular dynamics with coupling to an external bath. *J. Chem. Phys.*, **81**, 3684–3690.

Bevilacqua,M., Butcher,E., Furie,B., Gallatin,M., Gimbrone,M., Harlan,J., Kishimoto,K., Lasky,L. and McEver,R. (1991) Selectins: a family of adhesion receptors. *Cell*, **67**, 233.

Billeter,M., Riek,R., Wider,G., Hornemann,S., Glockshuber,R. and Wüthrich,K. (1997) Prion protein NMR structure and species barrier for prion diseases. *Proc. Natl. Acad. Sci. USA*, **94**, 7281–7285.

Capellari,S., Zaidi,S.I.A., Urig,C.B., Perry,G., Smith,M.A. and Petersen,R.B. (1999) Prion protein glycosylation is sensitive to redox change. *J. Biol. Chem.*, **274**, 34846–34850.

Case,D.A., Pearlman,D.A., Caldwell,J.W., Cheatham,T.E., Ross,W.S., Simmerling,C.L., Darden,T.A., Merz,K.M., Stanton,R.V., Cheng,A.L. and others. (1997) AMBER 5, University of California, San Francisco.

Caughey,B., Race,R.E., Ernst,D., Buchmeier,M.J. and Chesebro,B. (1989) Prion protein biosynthesis in scrapie-infected and uninfected neuroblastoma cells. *J. Virol.*, **63**, 175–181.

Collinge,J., Sidle,K.C., Meads,J., Ironside,J. and Hill,A.F. (1996) Molecular analysis of prion strain variation and the aetiology of 'new variant' CJD. *Nature*, **383**, 685–690.

Cornell,W.D., Cieplak,P., Bayly,C.I. and Kollman,P.A. (1993) Application of RESP charges to calculate conformational energies, hydrogen bond energies and free energies of solvation. *J. Am. Chem. Soc.*, **115**, 9620–9631.

Cornell,W.D., Cieplak,P., Bayly,C.I., Gould,I.R., Merz,K.M., Ferguson,D.M., Spellmeyer,D.C., Fox,T., Caldwell,J.W. and Kollman,P.A. (1995) A second generation force field for the simulation of proteins, nucleic acids and organic molecules. *J. Am. Chem. Soc.*, **117**, 5179–5197.

Darden,T., York,D. and Pedersen,L. (1993) Particle mesh Ewald: a N · log (N) method for Ewald sums in large systems. *J. Chem. Phys.*, **98**, 10089–10092.

Daude,N., Lehmann,S. and Harris,D.A. (1997) Identification of intermediate steps in the conversion of a mutant prion protein to a scrapie-like form in cultured cells. *J. Biol. Chem.*, **272**, 11604–11612.

Donne,D.G., Viles,J.H., Groth,D., Mehlhorn,I., James,T.L., Cohen,F.E., Prusiner,S.B., Wright,P.E. and Dyson,H.J. (1997) Structure of the recombinant full-length hamster prion protein PrP (29- 231): the N terminus is highly flexible. *Proc. Natl. Acad. Sci. USA*, **94**, 13452–13457.

Edenhofer,F., Weiss,S., Winnacker,E.L. and Famulok,M. (1997) Chemistry and molecular biology of transmissible spongiform encephalopathies. *Angew. Chem. Int. Ed. Engl.,* **36**, 1675–1694.

Eggens,I., Fenderson,B., Toyokuni,T., Dean,B., Stroud,M. and Hakomori,S. (1989) Specific interaction between Lex and Lex determinants. A possible basis for cell recognition in preimplantation embryos and in embryonal carcinoma cells. *J. Biol. Chem.*, **264**, 9476–9484.

Endo,T., Groth,D., Prusiner,S. and Kobata,A. (1989) Diversity of oligosaccharide structures linked to asparagines of the scrapie prion protein. *Biochemistry*, **28**, 8380–8388.

Ferguson,M.A. (1992) Glycosyl-phosphatidylinositol membrane anchors: the tale of a tail. *Biochem. Soc. Trans.*, **20**, 243–256.

Friedrichson,T. and Kurzchalia,T.V. (1998) Microdomains of GPI-anchored proteins in living cells revealed by crosslinking. *Nature*, **394**, 802–805.

Frisch,M.J., Trucks,G.W., Schlegel,H.B., Gill,P.M.W., Robb,M.A., Cheeseman,J.R., Keith,T.A., Petersson,G.A., Montgomery,J.A., Raghavachari,K. and others. (1994) Gaussian 94, Revision E.1. Gaussian Inc., Pittsburgh, PA.

Gilson,M.K. and Honig,B.H. (1987) Calculation of electrostatic potentials in an enzyme active site. *Nature*, **330**, 84–86.

Haraguchi,T., Fisher,S., Olofsson,S., Endo,T., Groth,D., Tarentino,A., Borchelt,D.R., Teplow,D., Hood,L., Burlingame,A. and others. (1989) Asparagine-linked glycosylation of the scrapie and cellular prion proteins. *Arch. Biochem. Biophys.*, **274**, 1–13.

Harris,D.A. (1999) Cellular biology of prion diseases. Clin. *Microbiol. Rev.*, **12**, 429–444.

Hedge,R.S., Mastrianni,J.A., Scott,M.R., DeFea,K.A., Tremblay,P., Torchia,M., DeArmond,S.J., Prusiner,S.B. and Lingappa,V.R. (1998) A transmembrane form of the prion protein in neurodegenerative disease. *Science*, **279**, 827–834.

Hill,A.F., Desbruslais,M., Joiner,S., Sidle,K.C., Gowland,I., Collinge,J., Doey,L.J. and Lantos,P. (1997) The same prion strain causes vCJD and BSE. *Nature*, **389**, 448–450.

Homans,S.W., Edge,C.J., Ferguson,M.A., Dwek,R.A. and Rademacher,T.W. (1989) Solution structure of the glycosylphosphatidylinositol membrane anchor glycan of *Trypanosoma brucei* variant surface glycoprotein. *Biochemistry*, **28**, 2881–2887.

Horiuchi,M. and Caughey,B. (1999) Specific binding of normal prion protein to the scrapie form via a localized domain initiates its conversion to the protease-resistant state. *EMBO J.*, **18**, 3193–3203.

Horwich,A. and Weissman,J. (1997) Deadly conformations—protein misfolding in prion disease. *Cell*, **89**, 499–510.

Hosszu,L.L.P., Baxter,N.J., Jackson,G.S., Power,A., Clarke,A.R., Waltho,J.P., Craven,C.J. and Collinge,J. (1999) Structural mobility of the human prion protein probed by backbone hydrogen exchange. *Nature Struct. Biol.*, **6**, 740–743.

Huang,Z., Prusiner,S.B. and Cohen,F.E. (1996) Scrapie prions: a three-dimensional model of an infectious fragment. *Fold. Des.*, **1**, 13–19.

Ironside,J.W. (1998) Prion diseases in man. *J. Pathol.*, **186**, 227–234.

James,T., Liu,H., Ulyanov,N., Farr-Jones,S., Zhang,H., Donne,D., Kaneko,K., Groth,D., Mehlhorn,I., Prusiner,S. and Cohen,F. (1997) Solution structure of a 142-residue recombinant prion protein corresponding to the infectious fragment of the scrapie isoform. *Proc. Natl. Acad. Sci. USA*, **94**, 10086–10091.

Jorgensen,W.L., Chandrasekhar,J., Madura,J.D., Impey,R.W. and Klein,M.L. (1983) Comparison of simple potential functions for simulating liquid water. *J. Chem. Phys.,* **79**, 926–935.

Kabsch,W. and Sander,C. (1983) Dictionary of protein secondary structure: pattern recognition of hydrogen-bonded and geometrical features. *Biopolymers*, **22**, 2577–2637.

Kaneko,K., Zulianello,L., Scott,M., Cooper,C.M., Wallace,A.C., James,T.L., Cohen,F.E. and Prusiner,S.B. (1997a) Evidence for protein X binding to a discontinuous epitope on the cellular prion protein during scrapie prion propagation. *Proc. Natl. Acad. Sci. USA*, **94**, 10069–10074.

Kaneko,K., Wille,H., Mehlhorn,I., Zhang,H., Ball,H., Cohen,F.E., Baldwin,M.A. and Prusiner,S.B. (1997b) Molecular properties of complexes formed between the prion protein and synthetic peptides. *J. Mol. Biol.*, **270**, 574–586.

Koradi,R., Billeter,M. and Wüthrich,K. (1996) MolMol. *J. Mol. Graphics*, **14**, 51–55.

Kocisko,D.A., Priola,S.A., Raymond,G.J., Chesebro,B., Lansbury,P.T. and Caughey,B. (1995) Species specificity in the cell-free conversion of prion protein to protease-resistant forms: a model for the scrapie species barrier. *Proc. Natl. Acad. Sci. USA*, **92**, 3923–3927.

Kraulis,P.J. (1991) MOLSCRIPT: A program to produce both detailed and schematic plots of protein structures. *J. Appl. Crystallogr.*, **24**, 946–950.

Lehmann,S. and Harris,D.A. (1997) Blockade of glycosylation promotes acquisition of scrapie-like properties by the prion protein in cultured cells. *J. Biol. Chem.*, **272**, 21479–21487.

Liu,H., Farr-Jones,S., Ulyanov,N.B., Llinas,M., Marqusee,S., Groth,D., Cohen,F.E., Prusiner,S.B. and James,T.L. (1999) Solution structure of syrian hamster prion protein rPrP (90–231). *Biochemistry*, **38**, 5362–5377.

Ma,J. and Lindquist,S. (1999) De novo generation of a PrPSc-like conformation in living cells. *Nature Cell. Biol.*, **1**, 358–361.

Mastrianni,J.A., Nixon,R., Layzer,R., Telling,G.C., Han,D., DeArmond,S.J. and Prusiner,S.B. (1999) Prion protein conformation in a patient with sporadic fatal insomnia. *N. Engl. J. Med.*, **340**, 1630–1638.

Maxfield,F. and Mayor,S. (1997) Cell surface dynamics of GPI-anchored proteins. *Adv. Exp. Med. Biol.*, **419**, 355–364.

McConville,M. and Ferguson,M.A.J. (1993) The structure, biosynthesis and function of glycosylated phosphatidylinositols in the parasitic protozoa and higher eukaryotes. *Biochem. J.*, **294**, 305–324.

Merritt,E.A. and Bacon,D.J. (1997) Raster3D: Photorealistic molecular graphics. *Methods Enzymol.*, **277**, 505–524.

Moore,R.C., Lee,I.Y., Silverman,G.L., Harrison,P.M., Strome,R., Heinrich,C., Karunaratne,A., Pasternak,S.H., Chishti,M.A., Liang,Y. and others. (1999) Ataxia in prion protein (PrP)-deficient mice is associated with upregulation of the novel PrP-like protein doppel. *J. Mol. Biol.*, **292**, 797–817.

Morillas,M., Swietnicki,W., Gambetti,P. and Surewicz,W.K. (1999) Membrane environment alters the conformational structure of the recombinant human prion protein. *J. Biol. Chem.*, **274**, 36859–36865.

Morrissey,M.P. and Shakhnovich,E.I. (1999) Evidence for the role of PrP (C) helix 1 in the hydrophilic seeding of prion aggregates. *Proc. Natl. Acad. Sci. USA*, **96**, 11293–11298.

Muramoto,T., Scott,M., Cohen,F.E. and Prusiner,S.B. (1996) Recombinant scrapie-like prion protein of 106 amino acids is soluble. *Proc. Natl. Acad. Sci. USA*, **93**, 15457–15462.

Naidoo,K.J., Denysyk,D. and Brady,J.W. (1997) Molecular dynamics simulations of the N-linked oligosaccharide of the lectin from Erythrina corallodendron. *Protein Eng.*, **10**, 1249–1261.

Pan,K.M., Baldwin,M., Nguyen,J., Gasset,M., Serban,A., Groth,D., Mehlhorn,I., Huang,Z., Fletterick,R.J., Cohen,F.E. and Prusiner,S.B. (1993) Conversion of a-helices into b-sheets features in the formation of the scrapie prion proteins. *Proc. Natl. Acad. Sci. USA*, **90**, 10962–19666.

Pearlman,D.A., Case,D.A., Caldwell,J.W., Ross,W.S., Cheatham,T.E., DeBolt,S., Ferguson,D.M., Seibel,G. and Kollman,P.A. (1995) AMBER, a package of computer programs for applying molecular mechanics, normal mode analysis, molecular dynamics and free energy calculations to simulate the structural and energetic properties of molecules. *Comp. Phys. Commun.*, **91**, 1–41.

Peters,T. and Pinto,B.M. (1996) Structure and dynamics of oligosaccharides: NMR and modeling studies. *Curr. Opin. Struct. Biol.*, **6**, 710–720.

Petersen,M.T., Martel,P., Petersen,E.I., Drablos,F. and Petersen,S.B. (1997) Surface and electrostatics of cutinases. *Methods Enzymol.*, **284**, 130–154.

Petersen,R.B., Parchi,P., Richardson,S.L., Urig,C.B. and Gambetti,P. (1996) Effect of the D178N mutation and the codon 129 polymorphism on the metabolism of the prion protein. *J. Biol. Chem.*, **271**, 12661–12668.

Priola,S.A., Caughey,B., Wehrly,K. and Chesebro,B. (1995) A 60-kDa prion protein (PrP) with properties of both the normal and scrapie-associated forms of PrP. *J. Biol. Chem.*, **270**, 3299–3305.

Prusiner,S.B. (1982) Novel proteinaceous infectious particles cause scrapie. *Science*, **216**, 136–144.

Prusiner,S.B. (1991) Molecular biology of prion diseases. *Science*, **252**, 1515–1522.

Prusiner,S.B. (1996) Prions. In Fields,B.N., Knipe,D.M. and Howley,P.M. (eds.), *Fields Virology*. Lippincott-Raven, Philadelphia, pp. 2901–2950.

Prusiner,S.B. (1998) Prions. *Proc. Natl. Acad. Sci. USA*, **95**, 13363–13383.

Riek,R., Hornemann,S., Wider,G., Billeter,M., Glockshuber,R. and Wüthrich,K. (1996) NMR structure of the mouse prion protein domain PrP (121–231). *Nature*, **382**, 180–182.

Riek,R., Hornemann,S., Wider,G., Glockshuber,R. and Wüthrich,K. (1997) NMR characterization of the full-length recombinant murine prion protein, mPrP (23–231). *FEBS Lett.*, **413**, 282–288.

Riek,R., Wider,G., Billeter,M., Hornemann,S. and Glockshuber,R. (1998) Prion protein NMR structure and familial human spongiform encephalopathies. *Proc. Natl. Acad. Sci. USA*, **95**, 11667–11172.

Rogers,M., Taraboulos,A., Scott,M., Groth,D. and Prusiner,S.B. (1990) Intracellular accumulation of the cellular prion protein after mutagenesis of its Asn-linked glycosylation sites. *Glycobiology*, **1**, 101–109.

Rudd,P.M., Endo,T., Colominas,C., Groth,D., Wheeler,S.F., Harvey,D.J., Wormald,M.R., Serban,H., Prusiner,S.B., Kobata,A. and Dwek,R.A. (1999a) Glycosylation differences between the normal and pathogenic prion protein isoforms. *Proc. Natl. Acad. Sci. USA*, **96**, 13044–13049.

Rudd,P.M., Wormald,M.R., Stanfield,R.L., Huang,M., Mattsson,N., Speir,J.A., DiGennaro,J.A., Fetrow,J.S., Dwek,R.A. and Wilson,I.A. (1999b) Roles for glycosylation of cell surface receptors involved in cellular immune recognition. *J. Mol. Biol.*, **293**, 351–366.

Rudd,P.M., Wormald,M.R., Harvey,D.J., Devasahayam,M., McAlister,M.S., Brown,M.H., Davis,S.J., Barclay,A.N. and Dwek,R.A. (1999c) Oligosaccharide analysis and molecular modeling of soluble forms of glycoproteins belonging to the Ly-**6**, scavenger receptor and immunoglobulin superfamilies expressed in Chinese hamster ovary cells. *Glycobiology*, **9**, 443–458.

Safar,J., Wille,H., Itri,V., Groth,D., Serban,H., Torchia,M., Cohen,F.E. and Prusiner,S.B. (1998) Eight prion strains have PrP (Sc) molecules with different conformations. *Nature Med.*, **4**, 1157–1165.

Schätzl,H.M., Da Costa,M., Taylor,L., Cohen,F.E., Prusiner,S.B. and Tateishi,J. (1995) Prion protein gene variation among primates. *J. Mol. Biol.*, **245**, 362–374.

Shyng,S.L., Huber,M.T. and Harris,D.A. (1993) A prion protein cycles between the cell surface and an endocytic compartment in cultured neuroblastoma cells. *J. Biol. Chem.*, **268**, 15922–15928.

Somerville,R.A. (1999) Host and transmissible spongiform encephalopathy agent strain control glycosylation of PrP. *J. Gen. Virol.*, **80**, 1865–1872.

Stahl,N., Borchelt,D.R., Hsiao,K. and Prusiner,S.B. (1987) Scrapie prion protein contains a phosphatidylinositol glycolipid. *Cell*, **51**, 229–240.

Stahl,N., Baldwin,M.A., Hecker,R., Pan,K.M., Burlingame,A.L. and Prusiner,S.B. (1992) Glycosylinositol phospholipid anchors of the scrapie and cellular prion proteins contain sialic acid. *Biochemistry*, **31**, 5043–5053.

Stimson,E., Hope,J., Chong,A. and Burlingame,A.L. (1999) Site-specific characterization of the N-linked glycans of murine prion protein by high-performance liquid chromatography/electrospray mass spectrometry and exoglycosidase digestions. *Biochemistry*, **38**, 4885–4895.

Telling,G.C., Scott,M., Mastrianni,J., Gabizon,R., Torchia,M., Cohen,F.E., DeArmond,S.J. and Prusiner,S.B. (1995) Prion propagation in mice expressing human and chimeric PrP transgenes implicates the interaction of cellular PrP with another protein. *Cell*, **83**, 79–90.

Varki,A. (1993) Biological roles of oligosaccharides: all of the theories are correct. *Glycobiology*, **3**, 97–130.

Varma,R. and Mayor,S. (1998) GPI-anchored proteins are organized in submicron domains at the cell surface. *Nature*, **394**, 798–801.

Vaughan,L. (1996) Signal transduction by GPI-anchored receptors in the nervous system. *Sem. Neurosci.*, **8**, 397–403.

Vey,M., Pilkuhn,S., Wille,H., Nixon,R., DeArmond,S.J., Smart,E.J., Anderson,R.G., Taraboulos,A. and Prusiner,S.B. (1996) Subcellular colocalization of the cellular and scrapie prion proteins in caveolae-like membranous domains. *Proc. Natl. Acad. Sci. USA*, **93**, 14945–14949.

Wadsworth,J.D.F., Hill,A.F., Joiner,S., Jackson,G.S., Clarke,A.R. and Collinge,J. (1999) Strain-specific prion-protein conformation determined by metal ions. *Nature Cell Biol.*, **1**, 55–59.

Warwicker,J. (1997) Species barriers in a model for specific prion protein dimerization. *Biochem. Biophys. Res. Commun.*, **232**, 508–512.

Weiner,S.J., Kollman,P.A., Nguyen,D.T. and Case,D.A. (1986) An all atom force field for simulations of proteins and nucleic acids. *J. Comput. Chem.*, **7**, 230–252.

Weller,C.T., McConville,M. and Homans,S.W. (1994) Solution structure and dynamics of a glycoinositol phospholipid (GIPL-6) from Leishmania major. *Biopolymers*, **34**, 1155–1163.

Wildegger,G., Liemann,S. and Glockshuber,R. (1999) Extremely rapid folding of the C-terminal domain of the prion protein without kinetic intermediates. *Nat. Struct. Biol.*, **6**, 550–553.

Woods,R.J., Dwek,R.A., Raymond,A. and Edge,C.J. (1995) Molecular mechanical and molecular dynamical simulations of glycoproteins and oligosaccharides. 1. GLYCAM_93 parameter development. *J. Phys. Chem.*, **99**, 3832–3846.

Yanai,A., Meiner,Z., Gahali,I., Gabizon,R. and Taraboulos,A. (1999) Subcellular trafficking abnormalities of a prion protein with a disrupted disulfide loop. *FEBS Lett.*, **460**, 11–16.

Zahn,R., Liu,A., Lührs,T., Riek,R., von Schrotter,C., López,F., Billeter,M., Calzolai,L., Wider,G. and Wüthrich,K. (2000) NMR solution structure of the human prion protein. *Proc. Natl. Acad. Sci. USA*, **97**, 145–150.

Zuegg,J. and Gready,J.E. (1999) Molecular dynamics simulations of human prion protein: importance of correct treatment of electrostatic interactions. *Biochemistry*, **38**, 13862–13876.